Analysis of the Magnetic Exchange Interactions in Yttrium(III) Complexes Containing Nitronyl Nitroxide Radicals

Julie Jung, Marin Puget, Olivier Cador, Kevin Bernot, Carmen J. Calzado, Boris Le Guennic

Analysis of the Magnetic Exchange Interactions in Yttrium(III) Complexes Containing Nitronyl Nitroxide Radicals

Julie Jung,[†,‡] Marin Puget,[¶] Olivier Cador,[†] Kevin Bernot,[*,¶] Carmen J. Calzado,[*,§] and Boris Le Guennic[*,†]

Institut des Sciences Chimiques de Rennes, UMR 6226 CNRS, Université de Rennes 1, 263 Avenue du Général Leclerc, 35042 Cedex Rennes, France, Max Planck Institut für Chemische Energiekonversion, Stiftstr. 34-36, D-45470 Mülheim an der Ruhr, Germany, INSA, Institut des Sciences Chimiques de Rennes UMR CNRS 6226, 35708 Rennes, France, and Departamento de Química Física. Universidad de Sevilla. c/ Prof. García González, s/n. 41012 Sevilla, Spain

E-mail: kevin.bernot@insa-rennes.fr; calzado@us.es; boris.leguennic@univ-rennes1.fr

Abstract

We report a combined theoretical and experimental investigation of the exchange interactions governing the magnetic behavior of a series of nitronyl-nitroxide (NIT)-based Y(III) complexes, *i.e.* Y(hfac)$_3$(NIT-R)$_2$ with R = PhOPh (**1**), PhOEt (**2**) and PhOMe (**3a**, **3b**). Even if some of these complexes or their Dy(III) parents were already described in the literature [Zhao et al. *Trans. Met. Chem.* **2006**, *31*, 593; Bernot et

---

[*]To whom correspondence should be addressed
[†]Université de Rennes
[‡]Present address: Max Planck Institut für Chemische Energiekonversion
[¶]INSA de Rennes
[§]Universidad de Sevilla

al. *J. Am. Chem. Soc.* **2009**, *131*, 5573], their synthesis procedure as well as their structural and magnetic properties were completely reconsidered. Depending on the nature of R and of crystallization conditions, $Y(hfac)_3(NIT-R)_2$ units can be organized as supramolecular dimers, linear or orthogonal chains. Such structural diversity within the series induces extremely different magnetic behaviors. The observed behaviors are rationalized by state-of-the-art wave-function-based quantum chemical approaches (CASSCF/DDCI) that demonstrate the existence of effective intra-molecular interactions between the NIT-R radical ligands of an isolated $Y(hfac)_3(NIT-R)_2$ molecule, but also between NIT-R moieties belonging to different $Y(hfac)_3(NIT-R)_2$ units. These results are supported by the use of spin Hamiltonian models going beyond the basic Bleaney-Bowers formalism to properly fit the experimental magnetic data. Finally, the microscopic mechanisms behind the evidenced intramolecular exchange interactions are elucidated through the inspection of the calculated wave-function. In particular, whereas the role of Y orbitals was already proposed, we herein demonstrate the contribution of the $hfac^-$ ancillary ligands in mediating the magnetic interaction between the NIT radicals.

1. Introduction

Since the early 90's the magnetic behavior of isolated molecules has caught much attention.[1] The discovery of molecules that present magnetic bistability of molecular origin[2] made molecular magnetism emerge as an intense field of research.[3] In particular, Single Molecule Magnets (SMMs) have been evidenced as particularly suitable entities for information storage and processing,[4] spintronic,[5–8] or cryogenic[9] devices.

Basically, SMM behavior is achieved in molecules having both a strongly axial magnetic anisotropy and a high energy barrier to the reversal of their magnetic moment.[10,11] While the former property guarantees magnetic bistability by making the ground state a doublet and prevents fast relaxation in this doublet ground state by limiting the mixing between the two associated sub-states, the latter establishes the temperature window within which slow relaxation can be observed. Ultimately, the relaxation rate is only determined by the spin-phonon coupling mechanisms involved in the magnetic relaxation, which are completely system-dependent since correlated to the vibrations of both the molecule and the lattice.

The optimization of the performance of SMMs, especially the temperature window where they depict magnetic slow relaxation, can be achieved through different strategies. The first and simplest one consists in synthesizing poly-nuclear complexes[12] in order to increase the overall anisotropy of the molecule but the correlation between the anisotropy (D) and the total spin (S) of the molecule make this strategy hard to achieve[13] provided that the respective arrangement of the ions is carefully controlled.[14,15] A second approach is to use highly symmetrical and rigid ligands to carefully engineer ligand field and favor stabilization of ground-state magnetic moment along a defined axis.[16] This approach is particularly suitable for SMMs that use highly anisotropic lanthanide ions as spin carriers.[17] A third route is based on the use of isotopically-pure metal ion derivatives that avoid spontaneous loss of the magnetic bistability in zero-field.[18,19] Finally, a last strategy relies on the use of radical ligands that can induce strong magnetic exchange between anisotropic spin carriers.[20,21] One of the best examples of the latter strategy is given by the N_2^{3-} radical-bridged terbium(III)

complex by J. R. Long and coworkers,[22–24] which remains among the SMMs with the highest working temperature available to date.

Among well-known organic radicals, nitronyl-nitroxides (NIT) are particularly appealing since they allow to obtain edifices of various dimensionalities. In these architectures, significant magnetic coupling can be observed that induces 0-, 1-, 2- or 3-dimensional overall magnetic behaviors.[25–33] Such materials can also give rise to unique magnetic behavior such as next-nearest neighbor interactions,[34] one-dimensional helimagnetism[35–37] or Single Chain Magnets (SCMs) behavior.[38–40] Among the latter class of compounds, SCMs of formula $[Ln(hfac)_3(NIT-PhOPh)]_\infty$, where $hfac^-$ = hexafluoroacetylacetonate and NIT-PhOPh = 2,4'-benzoxo-4,4,5,5-tetramethyl-imi-dazoline-1-oxyl-3-oxide, were found to have a quite complex magnetic behavior[41] and deep investigation of their monomeric constitutive units was necessary for its rationalization.[42] From the pioneering work by Benelli, Caneschi and Gatteschi on the $Ln(hfac)_3(NIT-R)_2$ compounds, it appears that the coupling interaction between the lanthanide ion and the radical ligand (Ln–NIT) can be either ferromagnetic (FM) or antiferromagnetic (AFM) depending on the nature of the lanthanide ion while magnetic interaction between the two radical ligands (NIT–NIT) is always found antiferromagnetic.[25,34,43–48] Rationalization of these exchange interactions has been performed initially using angular overlap analysis.[25,46] On the basis of $Y(hfac)_3(NIT-R)_2$ investigations, three possible mechanisms for the NIT–NIT interaction have been proposed: (i) direct exchange, (ii) super-exchange through the metal ion and (iii) super-exchange through the non-radical hfac- ligands.[45–47] However, definitive validation of the magnetic coupling mechanisms in these relatively simple units is still lacking. This is due, on the one hand, to the peculiar electronic structure of the lanthanide ions that induces great variety of magnetic coupling mechanisms (isotropic and anisotropic exchange, dipolar coupling...)[49] and on the other hand, on the numerous exchange pathways potentially responsible for the overall magnetic behavior.

Fundamentally, magnetic exchange is related to electronic repulsion and more precisely

to the Fermi hole surrounding the electrons. This interaction is thus mediated through electronic spin.[49] From the computational point of view, as for magnetic anisotropy or ligand-field effects,[50–54] procedures to investigate magnetic exchange rely on the use of a model Hamiltonian which is derived either from chemical intuition or using the effective Hamiltonian theory.[55,56] In the simplest case, *i.e.* two half spins interacting isotropically, magnetic exchange can then be effectively described using the Heisenberg-Dirac-Van Vleck Hamiltonian. Yet, as soon as spin-orbit coupling (SOC) or local anisotropy arises, this Hamiltonian needs to be further refined,[57] which can complicate greatly the physical picture of the system. As a consequence, *ab initio* calculations can become quite intricate, especially for lanthanide-based complexes, where SOC and magnetic anisotropy are rather strong. The approach is further complicated since lanthanide ions interact rather poorly through magnetic exchange with other spin-carriers such as transition metals or organic radicals, with coupling constants not exceeding 10 cm^{-1}. This is mainly because the 4f shell of lanthanide trivalent ions is quite efficiently shielded by the outter 5s and 5d shells. This is the main reason why there are to date very few in-depth theoretical studies of magnetic exchange in lanthanide or more generally rare earth-based complexes.[58,59] For all these reasons, and as highlighted by Benelli and coworkers, an alternative approach consists in studying first magnetic exchange in diamagnetic derivatives such as Y(III), La(III) or Lu(III). Consequently, to disentangle all the relative contributions to magnetic exchange in the Ln(hfac)$_3$(NIT-R)$_2$ family, the complex Y(hfac)$_3$(NIT-PhOPh)$_2$ has been chosen as target compound for the present study.[42]

The magnetic behavior is then dominated by intramolecular interactions between the radicals. However, uncoordinated NO groups are known to bear non-negligible electronic density[60–62] and their respective geometric arrangement and distances in the crystal packing can give rise to sizeable intermolecular magnetic interactions (NIT$\cdots$NIT interactions) that may compete with the intramolecular (NIT–NIT) ones. We have thus chosen to use different substituents on the aliphatic group of the nitronyl-nitroxide radical to afford structural diversity to our study. Three different substitutions in *para* position of the phenyl ring have

5

been explored affording three derivatives of formula Y(hfac)$_3$(NIT-R)$_2$ with R = PhOPh (**1**), PhOEt (**2**)[42] and PhOMe (**3a**,[63] **3b**) (Scheme 1). They present very different supramolecular architectures, from dimers to linear or orthogonal chains, with a wide range of intermolecular distances (from 2.80 to 4.26 Å). Consequently, our study goes far beyond the investigation of SCM monomer's and a simple description of these systems through HDVV Hamiltonian. In fact, high level *ab initio* calculations provide a reliable qualitative and quantitative picture of the magnetic behavior. Moreover, insights on the microscopic mechanisms responsible for the through-yttrium magnetic interactions in this series of complexes are provided.
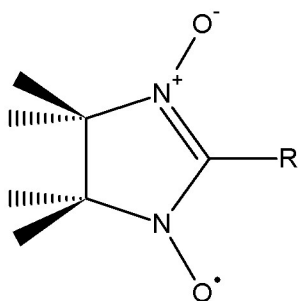
Scheme 1: Schematic representation of the nitronyl-nitroxide radical ligands used. Corresponding complexes of formula Y(hfac)$_3$(NIT-R)$_2$ for R = PhOPh, PhOEt and PhOMe are named **1**, **2**, **3a** and **3b**, respectively.

2. Experimental section

Synthesis and X-ray Crystallography

Crystallization procedures for Y(hfac)$_3$(NIT-R)$_2$ species vary drastically depending of both the nature of the -R substituent and the crystallization temperature (T$_{crist}$). For R = PhOPh, crystals could be obtained only for the Dy derivative (**1'**, CCDC-1519869). Powders of **1** are found isostructural to **1'** by comparison with their powder X-ray diffraction patterns (Figure S1). For R = PhOEt, only one species, **2**, is obtained whatever T$_{crist}$.[42] For R = PhOMe, if T$_{crist} < 5°$C, the already reported compound **3a** is mainly obtained (CCDC-178130),[63] whereas for T$_{crist} = 20°$C a majority of crystals of **3b** are found. Scanning of the

crystallization temperature conditions does not optimize the **3a**/**3b** ratio.

Single crystals of all derivatives were mounted on a APEXII AXS-Bruker diffractometer (150K) with Mo Kα radiation ($\lambda = 0.71073$ Å). Data reduction and cell refinement were performed with Denzo and Scalepack programs.[64] The crystal structures have been solved by direct methods using SIR97 program,[65] and refined with full matrix least-square methods based on F^2 (SHELX97)[66] with WINGX program.[67] All non-hydrogen atoms were refined anisotropically using SHELXL program. Hydrogen atoms bound to the organic ligand were located at ideal positions. Final structure refinement data of four derivatives are listed in Tables S1 and S2. Full details of the X-ray structure determination of the four crystal structures have been deposited at the Cambridge Crystallographic Data Center under the depository numbers CCDC-1519220 for **2** and CCDC-1519219 for **3b**. They can be obtained free of charge at http://www.ccdc.cam.ac.uk/conts/retrieving.html (or from the Cambridge Crystallographic Data Centre, 12, Union Road, Cambridge CB2 IEZ, UK; fax: (internat.) +44-1223/336-033; E mail: deposit@ccdc.cam.ac.uk), on request, from the authors and the reference to this publication.

Powder X-ray diffraction diagram of **1** has been collected at room temperature using a PanalyticalX'Pert Pro diffractometer equipped with an X'Celerator detector. Calculated pattern of **1'** was produced using Mercury 3.0 program.

Magnetic measurements

Magnetic measurements were performed on powder pellets with a MPMS Quantum Design magnetometer between 2 and 300K. All measurements have been corrected from sample holder contribution and from diamagnetic contributions as calculated by Pascal's constants.

Computational details

Ab initio calculations

All magnetic coupling constants have been evaluated by mean of Difference Dedicated Configuration Interaction (DDCI) calculations,[68,69] as implemented in the CASDI suite of programs.[70,71] The DDCI method is a multireference approach in which the wavefunction is defined by a combination of Slater determinants built from single and double excitations of the CASSCF wavefuntion. Contrary to the CASSCF approach only the wavefunction coefficients are optimised variationally in the DDCI method, making the calculation dependent on the initial set of orbitals. The excitations are organized according to the number of particles (p) and holes (h) they create in either the inactive or the virtual space, which gives rise to four different levels of calculation: (i) CASCI, which is the reference calculation with no excitations included, (ii) CAS+S, where only the 1h, 1p and 1h1p excitations are included, (iii) DDC2, where the 2h and 2p excitations are added, and (iv) DDCI, where the 2h1p and 1h2p excitations are also included.[55] Since the same set of MOs is used to described the different spin states of the system, the 2h2p excitations are not included because they do not change the relative energies of the states that are considered.[68,69]

In the end, the DDCI method is a very accurate variational approach for dynamical correlation, which has already been shown to be effective in quantitatively computing magnetic coupling constants in transition metal compounds of various dimensionalities but also in organic crystals.[55]

In this work, the common set of MOs is generated at the CASSCF level of theory. The MOs are then classified as active, occupied inactive and virtual orbitals, following their occupation in the reference CASSCF wavefunction. To decrease the computational cost, the core orbitals are not included in the DDCI calculations. The size of the active space (CAS(n,m) including n electrons in m orbitals) and the nature of the active orbitals are discussed more deeply in the Results and Discussion section. The CASSCF calculations and

the integral transformation from atomic to molecular basis sets have been performed with MOLCAS 7.6 code.[72]

Additionally, the mechanism of the magnetic coupling has been analyzed on the basis of EXSCI calculations, using the code developed by Maynau and coworkers.[73] The EXSCI method consists on the rational selection of the determinants employed to build the CI matrix using the exchange integral K_{ij} as a measure of the interaction between the orbitals involved in the excitations. The procedure requires the use of localized orbitals to make possible a safe truncation. Additionally, also the molecular integrals are truncated, retaining only those integrals larger than a certain threshold. The thresholds used in this work ($sli = 0.0003$, $sl1 = 0.001$, $sl2 = 0.0003$ in EXSCI and $sli1 = 0.001$, $sli2 = 0.0003$ for the molecular integrals) have been previously tested in other systems and are small enough to ensure that the relevant excitations are taken into account.

Structural models
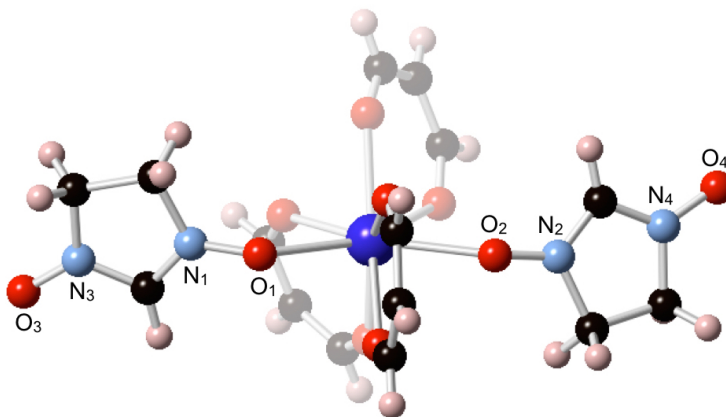
Figure 1: *NIT–Y–NIT* model for the *through-bond* NIT–NIT interaction in **1**. Black, light blue, red, light pink and dark blue spheres correspond to C, N, O, H and Y atoms, respectively.

For all complexes studied in this work, *ab initio* calculations were carried out on models built from the X-Ray structures of complexes **1**, **2**, **3a** and **3b**, without any further structural optimization. The model employed to study the *through-bond* NIT–NIT interactions, referred

9

hereafter as the *NIT–Y–NIT* model, is depicted in Figure 1. In this model, the CF_3 groups of the hfac$^-$ ligands are replaced by hydrogen atoms, as well as the -R group and the four methyl groups of each NIT radical ligand (respectively in positions -2-, -4- and -5- of the imidazole backbone). A fixed C–H distance of 0.93 Å (as in the hfac$^-$ ligand) is imposed to all created C–H bonds. These structural changes do not to lead to any significant change in the computed properties (see supporting information) whereas they significantly reduce the computational cost and speed-up the calculations.

For the *through-space* NIT$\cdots$NIT interactions, the so-called *NIT$\cdots$NIT* model only consists of two isolated NIT radical ligands kept in the same relative configuration as in the crystal. As for the *NIT–Y–NIT* model, the -R group and the four methyl groups of each NIT radical ligand are replaced by H atoms (except if explicitly notified in the text). We considered as much *NIT$\cdots$NIT* models as potential *through-space* interaction pathways. For instance, for **1**, we considered three possible *through-space* interaction pathways (Figure 6), with NIT$\cdots$NIT distances ranging from 3.7 Å to 8.9 Å, and thus, three *NIT$\cdots$NIT* models.

In the calculations, all atoms were described by ANO-RCC basis sets.[74–76] The following contractions were used: [7s6p4d1f] for the Y(III) ion, [4s3p1d] for the N and O atoms of NIT radical ligands and for the C atoms in between the two NO groups of each NIT ligand (position -2- of the imidazole backbone), [3s2p] for the remaining C, O and F (when included) atoms, and [2s] for the H atoms.

Spin Hamiltonian

Since the NIT radicals are isotropic half-spin carriers, the exchange interaction between two such ligands can be modeled using the Heisenberg-Dirac-Van Vleck (HDVV) hamiltonian written as follow:

$$\hat{H}_{HDVV} = -J\hat{S}_1 \cdot \hat{S}_2 \tag{1}$$

where $\hat{S}_1$ and $\hat{S}_2$ correspond to the spin operators of the two active sites, 1 and 2,

and J to the magnetic coupling constant between these sites. In this notation, the coupling constant equals the energy difference between the singlet and triplet states, $J = E(S) - E(T)$. For an antiferromagnetic interaction (*i.e.* singlet ground state) J is negative while for a ferromagnetic interaction (*i.e.* triplet ground state), J is positive. Here, one should recall that, intrinsically, exchange interactions are neither ferromagnetic or antiferromagnetic, but correspond to the contribution of several competing ferromagnetic and antiferromagnetic interactions, leading to an overall ferro- or antiferromagnetic behavior.[55,77–81]

3. Results and discussion

Crystal structures and magnetic properties

Compounds **1** and **3a** crystallize in the P2$_1$/n space group, whereas compounds **2**, and **3b** cristallize in the P$\bar{1}$ and P2$_1$/c space groups, respectively (Tables S1 and S2). For all derivatives, the asymmetric unit is made of one Ln(hfac)$_3$ moiety coordinated to two different NIT radicals that act as monodentate ligands. A NIT–Ln–NIT molecule is then formed. The Ln^{3+} ion is coordinated by six oxygen atoms of three hfac$^-$ ligands and two oxygen atoms of the radical ligands to form a fully oxygenated environment (LnO$_8$) close to a triangular dodecahedron (D$_{2d}$ site symmetry) (Table S3). All derivatives show similar Ln-O distances and O-Ln-O angles (Tables S4 and S5), and are of the same order of magnitude as in previously reported complexes of this kind.[42,45,63,82]

The substitution of the phenyl ring of the NIT radical has a huge effect on the organization of the molecule in the crystal packing (Figure 2). Compounds **2** and **3a** present the simplest crystal packing of the series with molecules that are related two-by-two through intermolecular interactions between the uncoordinated NO group of the radicals. However NO distances are quite different with 4.26 Å in **2** and 2.80 Å in **3a**. The formed supramolecular dimers are thus expected to present different magnetic behaviors. Compounds **1** and **3b** present more complex crystal packing as supramolecular chains are created by intermolecular
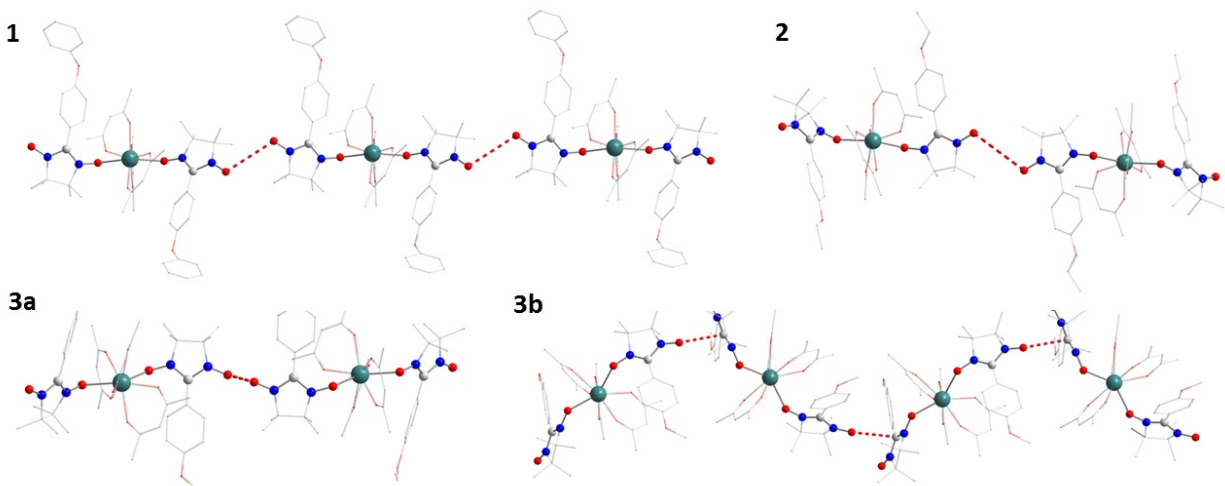
Figure 2: Representation of the $Y(hfac)_3(NIT-R)_2$ derivatives and their supramolecular arrangement (**1** and **3b**: chain-like structures; **2** and **3a** tetrameric-like structures). Shortest intermolecular distances (d_{inter}), either $O \cdots O$ or $O \cdots C$, as dashed red stick. **1**: $d_{inter} =$ 3.74 Å; **2**: $d_{inter} =$ 4.26 Å; **3a**: $d_{inter} =$ 2.80 Å; **3b**: $d_{inter} =$ 2.97 Å.

interactions between the NIT-Ln-NIT molecules. These latter entities can be thus considered as "monomers" of either a linear chain in the case of **1** or a zig-zag chain in **3b** that have a $[Y(hfac)_3(NIT-R)]_\infty$ formula.

This latter zig-zag chain shows a very peculiar orthogonal arrangement of the monomers that is possibly responsible of the unexpected reddish color of single crystals of **3b**. In fact, each non-coordinating NO group points at almost 90° of the imidazole plane of the neighboring radical and is quite close to central carbon of the ON–C–NO moiety (2.97 Å). This intermolecular interaction is expected to drastically modify the electronic delocalization within the radical. Finally, intermolecular $Ln \cdots Ln$ distances are 11.34 Å, 10.07 Å, 10.54 Å, 10.56 Å in **1**, **2**, **3a** and **3b**, respectively.

Magnetic measurements were performed on all complexes (see Experimental section for details). χ_M vs. T and $\chi_M T$ vs. T experimental curves, with χ_M the molar magnetic susceptibility ($cm^3 \, mol^{-1}$) and T the temperature in Kelvin, are shown in Figure 3. For **1** and **2**, the experimental susceptometry data are fitted on the basis of the Bleaney-Bowers
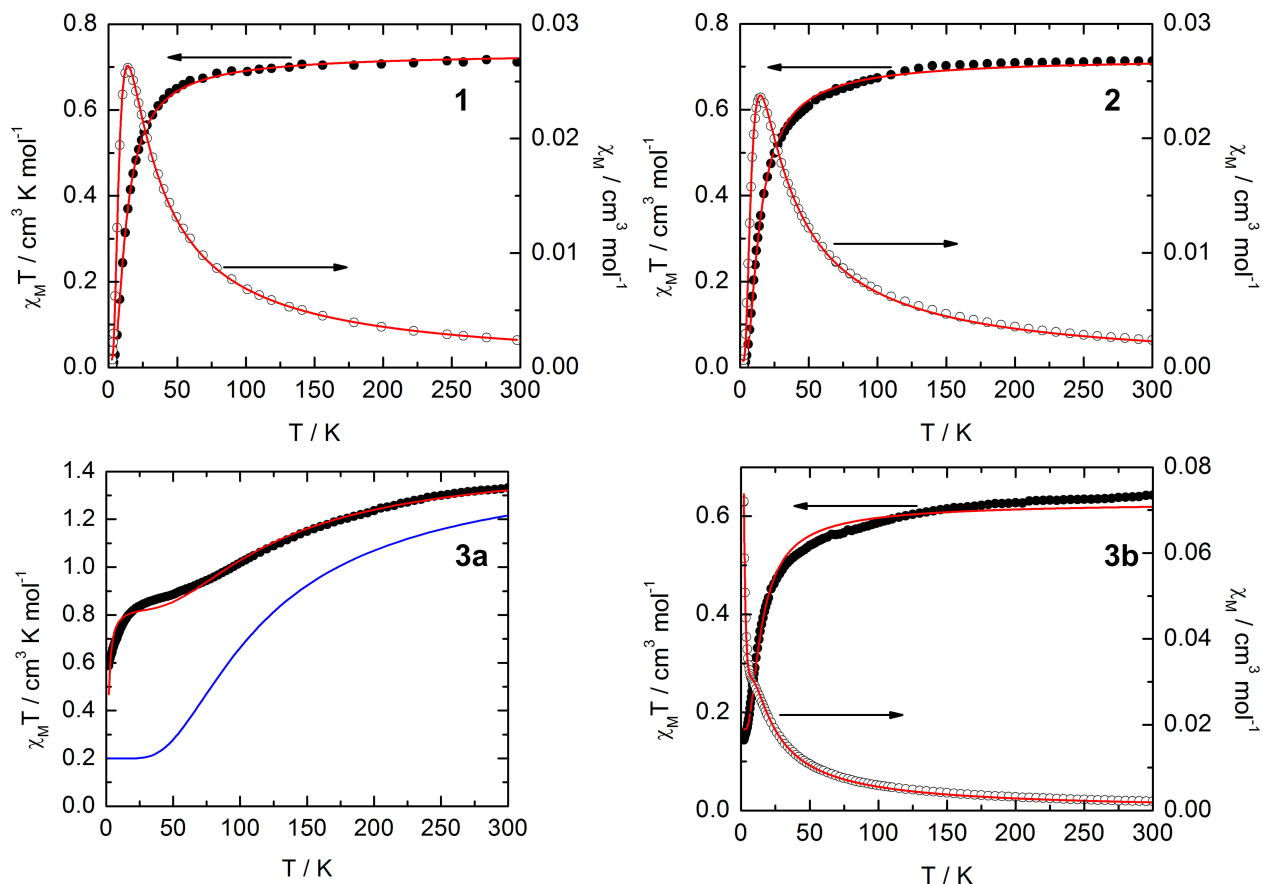
Figure 3: Temperature dependence of χ_M and $\chi_M T$ for all complexes. The red line corresponds to the best fitted curve. For **3a**, only the temperature dependence of $\chi_M T$ is given. The blue line is obtained if J_{bond} and J_{space} are inverted in the fitting procedure (see text).

Table 1: Magnetic data obtained from the best fits of χ_M vs. T and $\chi_M T$ vs. T curves for all complexes.

Compound	J_{bond} / cm^{-1}	J_{space} / cm^{-1}	g	$\%_{imp}$
1	-15.6	–	1.98	0.2
2	-16.5	–	1.93	0.8
3a	-24	-144	1.85	15.6
3b	-14.9	–	1.75	25.6

model:[1]

$$\chi_M = (1 - \%_{imp}) \frac{2Ng^2\beta^2}{kT(3 + exp(-J_{bond}/kT))} + \%_{imp}\frac{2Ng^2\beta^2}{3kT}s(s+1) \tag{2}$$

with J_{bond} the coupling constant between the two spins $(-J_{bond}\hat{s}_1 \cdot \hat{s}_2)$, N the Avogadro number, g the Zeeman factor, β the Bohr's magneton, k the Boltzmann constant, T the temperature and, finally $\%_{imp}$, the percentage of paramagnetic impurities with $s = 1/2$. The best fits (Figure 3) are obtained with values reported in Table 1 with an excellent agreement between experiments and the theoretical model. It shows that no *through-space* interaction between dimers are required to account for the observed behavior and that sizable interaction is mediated through Y(hfac)$_3$ moiety. For both compounds, the singlet-triplet gap is found about 16 cm^{-1}.[42] For **3b**, the same fitting procedure leads to poorer agreement with experiment since the sample appears to be contaminated by a relatively large amount of paramagnetic impurities (Figure 3, Table 1). Nevertheless, similar *through-bond* interaction is found (Table 1) between NIT–PhOMe radicals. It is important to mention at this stage that the Bleaney-Bowers model would be strictly identical if only *through-space* interactions were considered between radicals. However, since crystal packings of **1**, **2** and **3b** are different, the fact we extract nearly identical coupling constants certifies that the main interaction pathway is indeed the through–bond one.

Magnetic behavior of **3a** is erratic since on cooling from room temperature $\chi_M T$ reaches a plateau below 50 K before collapsing on further cooling (Figure 3). To explain such a behavior it is absolutely necessary to include more than one interaction term in the model. In other words, intermolecular interactions must be taken into account. Looking at the crystal structure it is reasonable to suppose that relatively large interactions propagate through the short intermolecular distance between two NIT ($d_{inter} = 2.8$ Å, Figure 2). In this frame the Hamiltonian that can be used is:

$$\hat{H} = -J_{bond}\hat{S}_1 \cdot \hat{S}_2 - J_{space}\hat{S}_2 \cdot \hat{S}_3 - J_{bond}\hat{S}_3 \cdot \hat{S}_4 \tag{3}$$

with J_{space} the *through-space* coupling constant. We are then considering a linear tetramer of coupled spins. The magnetic susceptibility can be calculated and then compared to experiment by numerical diagonalization of the Hamiltonian matrix. The best fit is represented on Figure 3 with parameters given in Table 1. Interestingly, J_{space} is still antiferromagnetic but one order of magnitude larger than J_{bond}, whereas the latter remains of the same order of magnitude than in the three previously discussed compounds. This strengthens our belief in the numerical approach we used. Furthermore, if one suppose that the role of the interactions should be inverted (the stronger within a dimer and the weaker between dimers), the blue curve on Figure 3 is obtained, that is far away from the experimental one. As for **3b**, a relatively large amount of paramagnetic impurities must be included to properly reproduce the experiment (Table 1). Since crystals of **3a** and **3b** have been collected by hands, we cannot discard the possibility of pollution of one sample by the other, and thus the larger the amount of **3a** in **3b** (and *vice et versa*), the smaller the g value.

Ab initio determination of the coupling constants for the NIT–NIT interactions in compound 1

Through-bond NIT–NIT interaction

An isolated NIT radical possesses three electrons in its valence shell, two of them occupying the antibonding π orbitals of the NO groups, and one the $2p_z$ orbital of the conjugated central C atom (Scheme 2). The combination of these local orbitals gives rise to three molecular orbitals (MOs), ϕ_b, ϕ_{SOMO} and ϕ_b^*, as represented in the right-hand side of Scheme 2. The distribution of the three valence electrons in these MOs gives a doublet ground state. As discussed elsewhere,[62,83,84] the largest contribution to the doublet wavefunction corresponds to the determinant with two electrons in the ϕ_b orbital and one unpaired electron occupying the ϕ_{SOMO} orbital.

Hence, the study of the interaction between two NIT radicals can be attempted at first
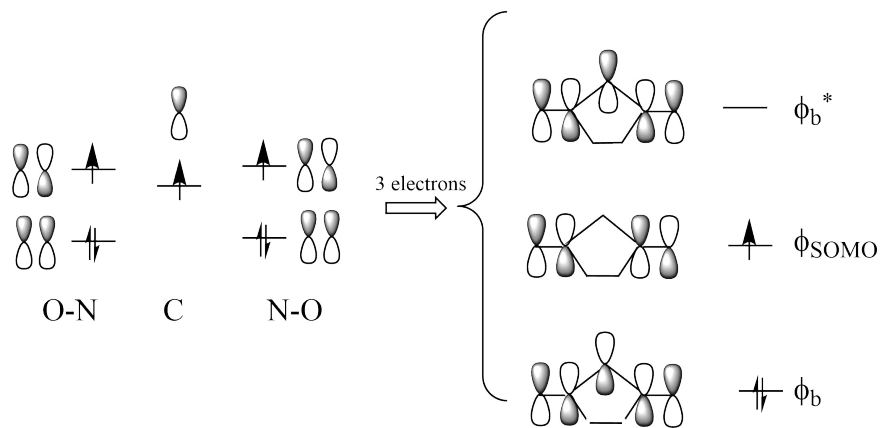
Scheme 2: Schematic representation of the π orbitals for an isolated NIT unit.[83]
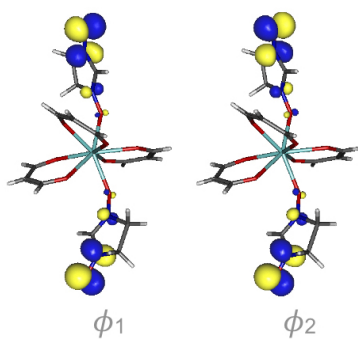
Figure 4: CAS(2/2)SCF MOs of the excited triplet state for the *NIT-Y-NIT* model in compound **1**.

using the minimal active space, with two unpaired electrons in the two ϕ_{SOMO} orbitals, *i.e.* a CAS(2/2). The active MOs are obtained from a CAS(2/2)SCF calculation on either the ground singlet state (S) or on the excited triplet state (T).

As shown in Figures 4 and S3, the active MOs correspond to the bonding (ϕ_1) and antibonding (ϕ_2) combinations of the ϕ_{SOMO} orbitals of each NIT group. They are almost identical for the (S) and (T) states, since in both cases, the electronic density is mostly localized on the external NO groups.

The J_{bond} values computed for the *through-bond* interaction with these two sets of orbitals are shown in Table 2. Even at the best level of calculation, the *ab initio* J_{bond} values are significantly smaller than that obtained from the fitting procedure. Such strong underestimation is particularly surprising at the DDCI level, where the key effects of dynamical correlation are taken into account and thus leading to J values in good agreement with the experimental values, at least in transition metal complexes.[55] However, this underestimation correlates well with the strong localization of the electron density on the external NO groups. Previous calculations on organic biradicals presented also this unusual behavior ,[62,83,85,86] and two different strategies have been adopted in the literature to overcome this problem: (i) to extend the active space by including all the valence π electrons and orbitals for each NIT radical, *i.e.* to use a CAS(6/6),[62,83,84] and (ii) to still rely on the minimal active space, but using an optimized set of MOs instead of the CASSCF ones which are excessively localized on the external NO moieties.[85,87–89] Here one should mention that increasing the quality of the basis sets, *i.e.* [4s3p1d] contraction for all C and O atoms (see Computational details), induces only a variation of $\sim 5\%$ of the calculated values.

Table 2 shows the results obtained when using the CAS(6/6) extended active space. As previously, the MOs employed in the CI calculations come from CAS(6/6)SCF calculations on either the singlet ground state or the triplet excited state. The six active MOs of the triplet state are shown in Figure 5. Similar shapes are found for the singlet MOs. Comparing with Figure 4, a larger electron delocalization on the central NO groups is observed, which

Table 2: Calculated magnetic coupling constants J_{bond} (cm^{-1}) for the *NIT–Y–NIT* model. In parenthesis, the values obtained with a CAS(2/2) using the CAS(6/6)SCF MOs. DDCI(6/6) values were not obtained due to computational limitations.

CAS		Singlet MOs	Triplet MOs	SA-7:3 singlet MOs	Natural DDCI MOs
(2/2)	CASCI	-0.4	-0.4	-1.8	-1.4
	CAS+S	-1.1	-1.1	-3.8	-4.4
	DDC2	-1.4	-1.2	-5.3	-5.9
	DDCI	-2.6	-2.4	-8.8	-7.9
(6/6)	CASCI	-0.7 (-1.3)	-1.0 (-1.3)		
	CAS+S	-1.7 (-1.8)	-2.1 (-2.6)		
	DDC2	-2.5 (-2.4)	-2.3 (-3.0)		
	DDCI	– (-4.2)	– (-4.0)		
J_{exp}			-15.6		

can be directly related to the improvement – with respect to the experimental value – of the calculated J_{bond} values. Nonetheless, the best estimate (*i.e.* -4.2 cm^{-1}) is still far of being quantitative since it only represents 25% of the experimental value. It is worth mention that this slight improvement is not related directly to the CAS extension itself but to the larger delocalization of the density observed in the two singly occupied MOs (ϕ_3 and ϕ_4 in the top of Figure 5), as demonstrated by the J_{bond} values in parenthesis in Table 2. It is also supported by the comparison between the spin density associated to the CAS(2/2) and CAS(6/6) triplet calculations (Figure S4). These J_{bond} values have been obtained on the basis of the CAS(6/6)SCF MOs, but including in the CI active space only the two singly occupied orbitals (*i.e.* orbitals ϕ_3 and ϕ_4). The present results strongly suggest that the failure of the CI calculation is not related to the size of the active space but to the quality of the MOs.

Thus, we decided to focus on optimizing the MOs within the frame of the minimal CAS. To this end, two options have been explored, both providing quite similar active MOs and hence close J_{bond} values (see Table 2). First, averaged natural orbitals were built from the density matrices of the singlet and triplet states at the DDCI(2/2) level. The resulting MOs are employed in subsequent DDCI calculations until convergence (iterative DDCI or IDDCI

18

(a) CAS(6/6)SCF singlet MOs

(b) Natural IDDCI(2/2) MOs

(c) CAS(2/2)SCF SA 7:3 singlet MOs
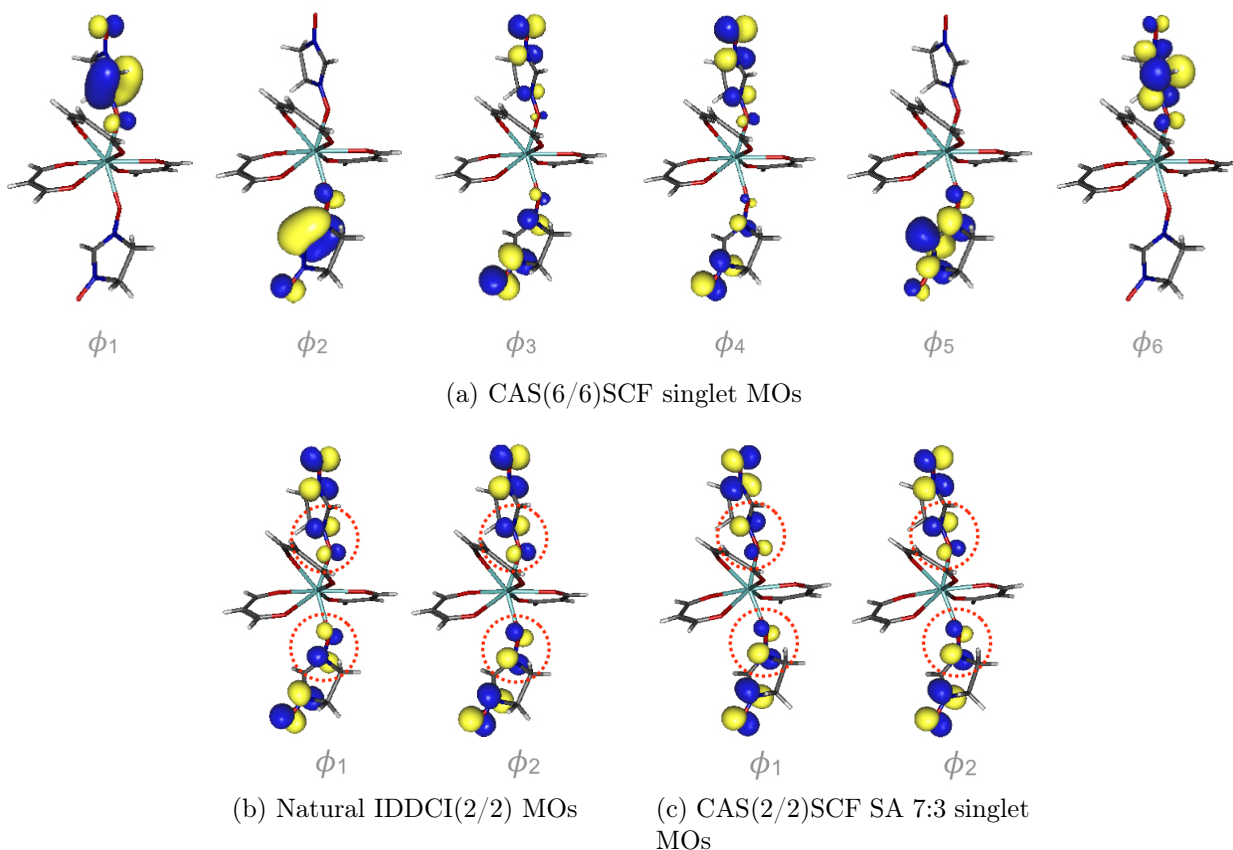
Figure 5: (a) CAS(6/6)SCF MOs of the triplet state for the *NIT–Y–NIT* model in compound **1** with occupations 1.89 (ϕ_1), 1.88 (ϕ_2), 1.00 (ϕ_3), 1.00 (ϕ_4), 0.11 (ϕ_5) and 0.12 (ϕ_6). ϕ_3 and ϕ_4 MOs correspond to the symmetric and antisymmetric combinations of the SOMO of each NIT radical. (b) Averaged natural orbitals from the density matrices of the singlet and triplet states at DDCI(2/2) level. (c) CAS(2/2)SCF MOs of the SA 7:3 singlet wavefunction for the *NIT–Y–NIT* model in compound **1**.

calculations).[90] This procedure has been shown to be efficient in eliminating any dependence of the DDCI results on the starting MOs, taking into account the orbital relaxation induced by the electron correlation. The shape of the so-obtained MOs is represented in Figure 5, the most relevant feature being the enhancement of the electron density on the central NO groups, which is in line with the increase of the calculated J_{bond} value at DDCI(2/2) level (Table 2). Alternatively, Angeli and Calzado have shown recently that it is possible to reproduce the natural DDCI magnetic orbitals with a simple state average CAS(2/2)SCF calculation, that mixes the singlet ground state (essentially represented by the neutral configuration, *i.e.* with one electron per magnetic site) and the excited ionic singlet states (the two active electrons on the same magnetic site).[87] This mixing induces the stabilization of the ionic states, which are usually too high in energy at the CASSCF level, allowing for the relaxation of the active orbitals, and thus providing a nice improvement of the calculated J values at MRPT2 level. In this previous work,[87,91] a 7:3 mixture of the neutral:ionic singlet states gave magnetic orbitals showing a large overlap with the DDCI natural MOs. The same mixture was used here and the so-obtained active orbitals are shown in Figure 5, with very similar features to those obtained from the IDDCI approach. The DDCI J_{bond} value with these SA-7:3 MOs (*i.e.* -8.8 cm^{-1}) is then closely similar to that obtained with the natural MOs (*i.e.* -7.9 cm^{-1}).

Unfortunately, there are no experimental data available with respect to the spin density in compound **1** or any other of the compounds investigated in the present work, which could validate the shape of the optimized magnetic MOs. Tentative polarized neutron diffraction (PND) measurements were carried out with no concluding results to date. However, for the free NIT radical and for $Cu(hfac)_2(NIT-Ph)_2$ compound, which can be seen as a Cu(II) analogue of compound **1**, such data are available.[60,61] In the former case, the spin density is equally delocalized on the two -NO groups of each NIT radical, while in the latter case, it is more delocalized on the outer -NO group of each NIT radical, with only a small contribution on the nitrogen atom of the -NO moiety linked to the Cu(II) ion. Since the Cu(II)

ion interacts rather strongly, *i.e.* covalently, with the NIT radical[61] while the Y(III)–NIT interaction is mainly electrostatic, one may expect that the spin density distribution in **1** is somewhere in between the two extreme pictures from the free NIT radical on one side and the Cu(hfac)$_2$(NIT-Ph)$_2$ compound on the other side. Thus, one may be confident in the distribution obtained either with natural or SA MOs (Figure 5b,c).

In the end, compared to the fitted J value (-15.6 cm^{-1}), our best *ab initio* estimate (-8.8 cm^{-1}) represents only 55% of this value, a notably larger deviation than expected for this method, which as already stated, cannot be attributed to the structural simplifications associated to the *NIT–Y–NIT* model (see Supporting Information).

Through-space NIT$\cdots$NIT interactions

The unexpected disagreement between the calculated and the fitted J values for **1** impels us to look for additional exchange interaction pathways able to explain the experimental thermal dependence of the susceptibility curve (Figure 3). Looking at the X-ray structure, three different *through-space* pathways are explored. They are illustrated in Figure 6. All of them involve two NIT radical groups coordinated to different but close Y(hfac)$_3$ moieties. In these three pathways, the NIT radical ligands are separated by 3.74 Å, 8.56 Å and 8.90 Å, respectively.

In the particular case of Pathway #2, to rule out any important contribution of the phenyl rings directly bound to the imidazole backbones to the exchange interaction through π-stacking interactions or electronic delocalization, two *NIT–NIT* models are considered: (i) the one classically used in this study (as described in Computational details) and (ii) a second one including explicitly these phenyl rings (one for each NIT radical ligand). The *through-space* NIT$\cdots$NIT interactions are evaluated using the approach that was most satisfactorily in the previous section, *i.e.* DDCI(2/2) on the basis of CASSCF SA-7:3 singlet MOs. For all pathways, the active orbitals correspond to the symmetric and antisymmetric combinations of the SOMOs of each NIT radical (Figure S5). As for the *through-bond*

(a) Pathway #1   (b) Pathway #2   (c) Pathway #3
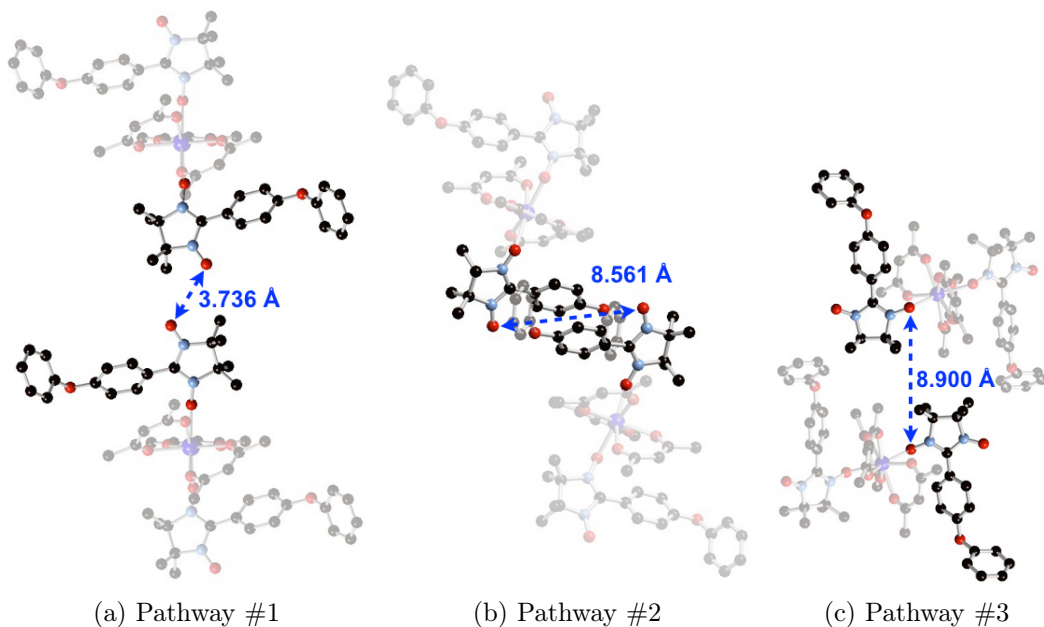
Figure 6: *Through-space* exchange pathways for **1**. Same color code as in Figure 1.

NIT–NIT interaction, using the CASSCF SA-7:3 singlet MOs allows for a better description of the magnetic orbitals, with almost equal electron delocalization over the two -NO groups of each NIT radical. For Pathways #2 (with and without the phenyl rings) and #3 the computed coupling constants are almost null (-0.0 cm^{-1} and +0.1 cm^{-1}, respectively), while for Pathway #1 the computed coupling constant results in a small but non-negligible anti-ferromagnetic interaction, with a J value of -3.6 cm^{-1}. First of all, these results prove the effectiveness of the *through-space* interactions pathways in the overall magnetic behavior of **1** since the intensity of the *through-space* NIT$\cdots$NIT interaction is more than 2/5 that of the *through-bond* NIT–NIT interaction. Though, the strength of the *through-space* NIT$\cdots$NIT interaction seems to decrease quite fast with increasing distance, since going from -3.6 cm^{-1} to zero while the NIT$\cdots$NIT distance goes from about 3.5 Å to about 8.5 Å.

Fitting of the susceptibility curves

The presence of a magnetic pathway (Pathway #1) connecting two neighbor NIT-Y(hfac)$_3$-NIT units questions the suitability of the Bleaney-Bowers model to fully represent the mag-

netic interactions in **1**, despite the high quality of the fitting based on this model (Figure 3). Indeed, in this model the magnetic behavior can only be attributed to isolated NIT-Y(hfac)$_3$-NIT units where the two NIT radicals are coupled antiferromagnetically, *i.e.* taking only into account the *through-bond* NIT–NIT interaction with $J = $ -15.6 cm^{-1}. On the other hand, the Hatfield model corresponds to a 1D magnetic chain with alternating exchange interactions decribed by two parameters J_1 and J_2, such as $J_2 = \alpha J_1$ (see Supporting Information).[1] The green curve in Figure 7 is obtained with this model using the calculated *through-bond* and *through-space* J values, *i.e.* $J_{bond} = $ -8.8 cm^{-1} and $J_{space} = $ -3.6 cm^{-1}, respectively, and α = 0.409. The fact that this curve predicts a larger χ value than the experimental one indicates that the magnetic interactions are underestimated in our computational protocol. By increasing these values by a factor of 1.5 (i.e. with J_{bond} and J_{space} raised to -13.2 cm^{-1} and -5.4 cm^{-1}, respectively) a better agreement with the experimental χ vs T curve is obtained (blue curve in Figure 7). This result suggests that, even at the DDCI level of calculation, the computed J values are underestimated by about 35%.
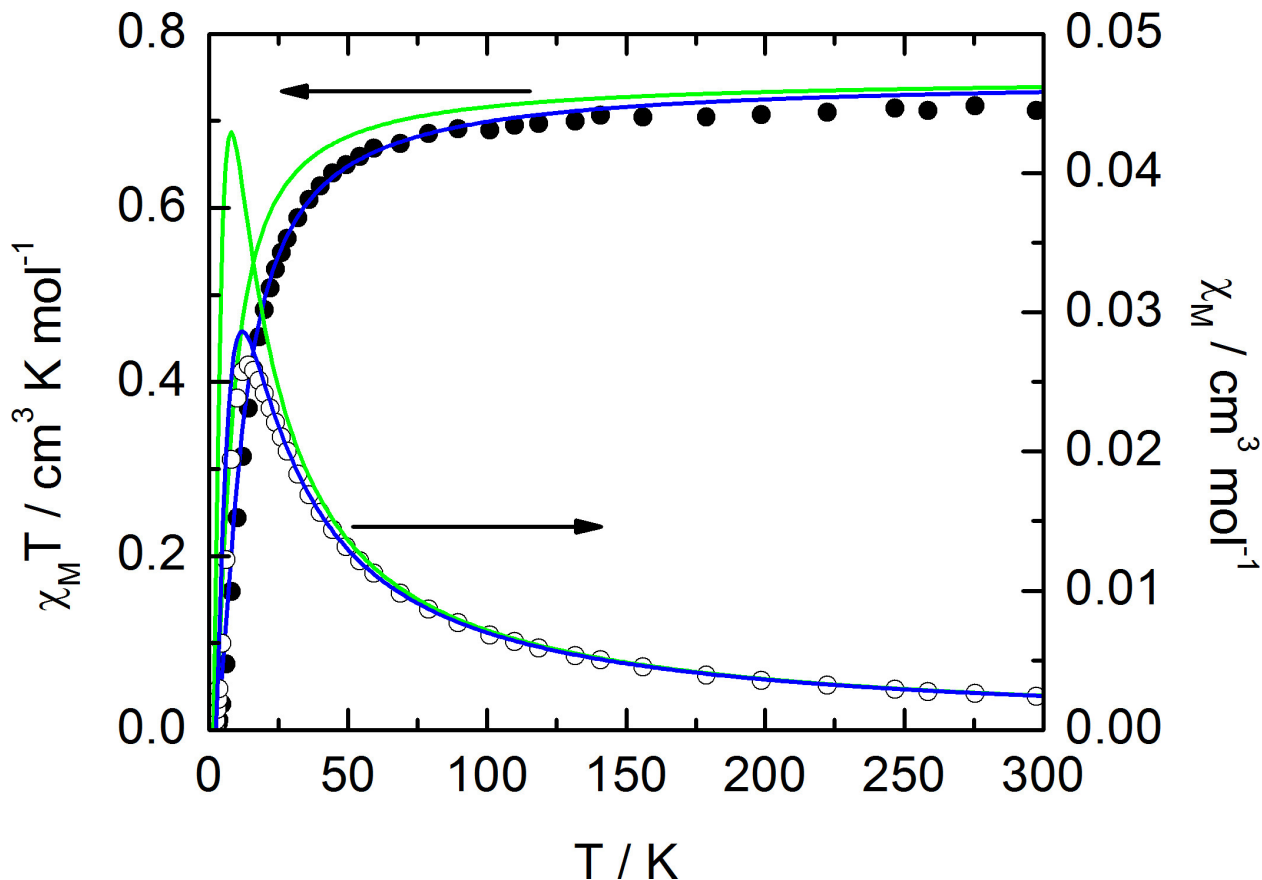
Figure 7: Plots of χ_M and $\chi_M T$ as a function of temperature for compound **1** with simulated curves using the Hatfield model and the calculated J values (green curve; J_{bond} = -8.8 cm^{-1}, J_{space} = -3.6 cm^{-1}) and $J * 1.5$ values (blue curve; J_{bond} = -13.2 cm^{-1} and J_{space} = -5.4 cm^{-1}). Both curves have been simulated using the experimental g value (g = 1.98).

To summarize, this result indicates that (i) for both the *through-bond* and *through-space* NIT–NIT interactions, the computed J values are underestimated; (ii) once the calculated J values are corrected, a model based on an alternating 1D chain can accurately reproduce the experimental dependence of the magnetic response with temperature; (iii) the Bleaney-Bowers model has to be considered as an effective model, able to reproduce the overall experimental behavior, but not as a realistic picture of the different interactions operating in **1**.

The Y(NO$_3$)$_3$(NIT-triazol)$_2$ compound

The underestimation of the J values in **1**, while puzzling, is not an isolated case. We have found the same trend for another NIT-based complex, *i.e.* the Y(NO$_3$)$_3$(NITtriazol)$_2$ (Figure S6) that has been investigated in-depth in the late 90's by Kahn[92,93] and Sutter.[94,95] Contrary to the other compounds investigated in the present work, in this complex, the NIT-derived radicals act as bidentate ligands. Also, the Y(III) ion is in a N$_2$O$_8$ environment, with six oxygen atoms coming from three 3 η^2-NO$_3$ ligands while the two remaining oxygen atoms and the two nitrogen atoms come from the two NIT-derived radical ligands. Finally, the large intermolecular NIT$\cdots$NIT distances (around 6 Å) suggests the absence of any *through-space* NIT$\cdots$NIT interaction. This is supported by the fit of the experimental data, which give an intermolecular interaction of 0.009 cm^{-1} when taken into account, whereas the experimental coupling constant of the *through-bond* NIT–NIT interaction is found at -3.1 cm^{-1}.[94] Using the same computational settings as previously and a *NIT–Y–NIT* model where all six methyl groups of each NIT-derived radical ligand are replaced by H atoms, the J value for the *through-bond* NIT–NIT interaction is computed (Table S7). Here again, the spin density, and thus the shape of the magnetic MOs (Figure S7), seem to be a key parameter in the calculated values. At the best level of calculation (DDCI(2/2) on the basis of SA-7:3 singlet MOs), the computed J_{bond} value (J_{bond} = -2.09 cm^{-1}) is again underestimated, by roughly 30% with respect to the experimental value. Till no opposite evidence has been given, one might thus consider this trend to be systematical for NIT-based complexes of this kind.

Mechanisms governing the coupling in Y(hfac)$_3$(NIT-PhOPh)$_2$ (1)

The mechanisms governing the NIT–NIT magnetic interaction through a rare earth ion, *i.e.* in the NIT-RE(hfac)$_3$-NIT complexes with RE = Gd(III), Eu(III), Y(III) have been addressed by different authors in the past.[25,27,45–47,96] Three main mechanisms have been invoked: (i) the direct interaction between NIT units, (ii) the super-exchange mediated by the hfac$^-$ ligands and (iii) the super-exchange mediated by the RE ion. In this latter case,

depending on the nature of the RE ion, different mechanisms have been suggested involving the highest occupied orbitals (4p for Y, 4f for Gd and Eu), virtual orbitals (4d and 5s for Y, 5d and 6s for Eu and Gd) or the partially occupied 4f orbitals for Gd and Eu ions.

In the particular case of the Y(III) complexes we are interested in, mechanism (i) can be eliminated due to the rather large distance between the NIT radicals (around 6 Å). For mechanism (ii), the p orbitals of the oxygen atoms belonging to the $hfac^-$ ligand perpendicular to the O_1-O_2 direction, later referred as central $hfac^-$ ligand (Figure 1), are assumed to be 90 degrees away from the magnetic MOs, which ensures significant orbital overlap, and thus a strong antiferromagnetic contribution (according to Goodenough and Kanamori's rules).[49] The same goes if one considers that the 4p orbitals of the Y(III) ion are involved. Finally, for mechanism (iii), super-exchange is expected to give an antiferromagnetic contribution through spin-polarisation in the empty 4d and/or 5s orbitals. In their inspiring work, Benelli and Gatteschi had a preference for the mechanisms involving either the occupied or the virtual orbitals of the Y(III) ion.[25,45] However, a definitive demonstration is still lacking.

With this in mind, we have used different strategies to elucidate the mechanism(s) actually operating in **1**, by isolating each of the effective mechanisms and estimating their contribution to the whole *through-bond* NIT–NIT interaction. In all these calculations, a minimal active space, *i.e.* DDCI(2/2), is employed based on the CASSCF SA-7:3 singlet MOs.

The contribution of direct exchange can be roughly evaluated using a simplified *NIT–Y–NIT* model where all the atoms of the three $hfac^-$ groups and the Y(III) ion are eliminated, *i.e.* only the two NIT radicals are considered, at the same distance and relative orientation as in the crystal structure. The J_{bond} value obtained at DDCI(2/2) level is of -0.1 cm^{-1}. This result confirms the hypothesis of Benelli *et al.*,[25,45] which ruled out this direct exchange mechanism due to the large intra-molecular NIT···NIT distances in these systems.

To analyze the role of the Y(III) ion and $hfac^-$ ligands in the super-exchange mechanisms, the whole set of CASSCF SA-7:3 MOs has been localized[97] and a new series of calculations

Table 3: Calculated magnetic coupling constants J_{bond} (cm^{-1}) for the *NIT–Y–NIT* model of complex **1** using localized orbitals and various orbital selections through the EXSCI approach. Reference value (without truncation) is J_{bond} = -8.9 cm^{-1}.

Selection	J_{bond}
whole set of orbitals	-7.2
without Y(III) orbitals	-6.4
without all hfac$^-$ orbitals	-4.9
without central hfac$^-$ orbitals	-5.2
without all hfac$^-$, Y(III) and occ. and virt. NIT π orbitals	-2.7

has been performed eliminating step-by-step the orbitals localized on these groups. The procedure benefits from the EXSCI approach, that considerably reduces the computational cost by excluding all the non-essential excitations by means of a threshold on the related exchange interaction integrals.[73] Details of this method and recent applications can be found in Refs. 73,98–101. Within the frame of the EXSCI approach, the reference J_{bond} value is now -7.2 cm^{-1} to be compared to -8.9 cm^{-1} obtained without truncation (Table 3). If all the orbitals centered on the Y(III) ion are eliminated, the J_{bond} value goes down to -6.4 cm^{-1}. This small reduction of J_{bond} excludes the super-exchange mechanism via the occupied 4p or virtual 4d or 5s orbitals of Y(III) ion as the main 'pathway' for the magnetic interaction. If instead, the orbitals centered on the three hfac$^-$ ligands are eliminated, the J_{bond} value goes down to -4.9 cm^{-1}, while if only the orbitals of the central hfac$^-$ ligand are eliminated J_{bond} = -5.2 cm^{-1} (Table 3). This clearly suggests the implication of the hfac$^-$ ligands in the super-exchange mechanism. In particular, the central hfac$^-$ actively participates to this mechanism (Scheme 3). Into more details, when looking at the DDCI wavefunction, it appears that the excited configurations with a significant weight can be described as charge transfer forms, related to the neutral ones by single excitations. In fact, as shown in Scheme 3, in the first step, one electron is promoted from one of the hfac$^-$ orbitals to the magnetic orbital located on one of the NIT radical. In other words, there is a charge transfer from the ancillary ligand to the NIT radical. Then, one electron from the second NIT radical

moves to the hfac⁻ orbital. This corresponds to the formation of an ionic form, where the two active electrons occupy simultaneously the same magnetic center. Next, one electron moves from the hfac⁻ ligand to the NIT radical, changing its spin. Finally, the neutral form is restored (Scheme 3). This mechanism is responsible for an antiferromagnetic contribution to the whole magnetic coupling, such as

$$J_{AF} \propto -4\frac{(t_{CT}^N)^2 \cdot (t_{CT}^I)^2}{\Delta E_{CT}^2 \cdot U} \tag{4}$$

where t_{CT}^N corresponds to the interaction between the charge transfer and the neutral form and t_{CT}^I is the interaction between the charge transfer and the ionic form. ΔE_{CT} and U are the relative energy of the CT and ionic forms, respectively (Scheme 3).[55,102–104]
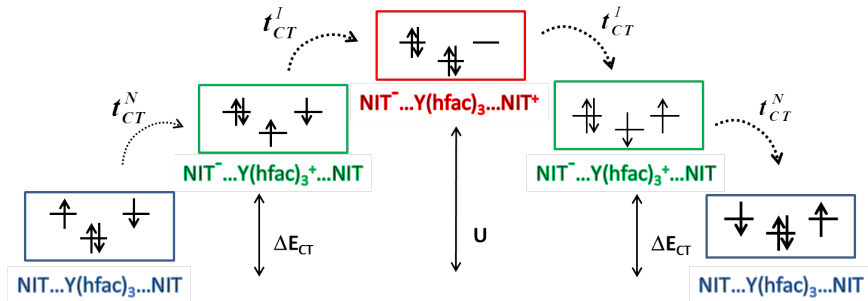
Scheme 3: Super-exchange mechanism involved in the *through-bond* NIT–NIT magnetic interaction in **1**: neutral (blue), ionic (red) and CT (green) forms.

If, in addition to the hfac⁻ and Y(III) orbitals, the occupied and virtual π orbitals centered on the NIT radicals (orbitals ϕ_1, ϕ_2, ϕ_5 and ϕ_6 in Figure 5) are eliminated, the J_{bond} value drops now to -2.7 cm⁻¹ (Table 3). These orbitals centered on the NIT radicals participate in the 1h1p excitations that promote one electron from the NIT occupied π orbital to the virtual π^* orbital, which contribute to the relaxation of the ionic and CT forms, reducing their energies ΔE_{CT} in Eq. 4. This provides an antiferromagnetic contribution to the overall magnetic coupling.

Furthermore, it is possible to isolate the effect of these 1h1p excitations by performing a *class-partitioned* CI calculation.[83,104–106] In this case, only a set of excitations is included

in the CI matrix. Its diagonalization gives the variational impact of the selected set of excitations on the coupling constant. The diagonalization of the CAS+1h1p space, that is, with only the CAS determinants (neutral and ionic forms) and the 1h1p excitation, gives a J_{bond} value of -5.6 cm^{-1} to be compared to the value obtained with the whole DDCI space, *i.e.* -8.9 cm^{-1}. The CAS+1h1p space represents about 40% of the whole DDCI space, meaning that the 1h1p excitations themselves bring an important contribution to the antiferromagnetic coupling constant, that is enhanced when interacting with the CT determinants in the DDCI space. Among the 1h1p excitations, those involving the π occupied and virtual MOs of the NIT radicals are the key ones. In fact, if the two occupied orbitals ϕ_1 and ϕ_2 (Figure 5) are eliminated, the J_{bond} value at the CAS+1h1p level is reduced to -0.7 cm^{-1} and finally becomes ferromagnetic with a value of +5.9 cm^{-1} at the DDCI level.

In summary, the subtle mechanism at the origin of the antiferromagnetic *through-bond* NIT-NIT interaction can be seen as a two-step mechanism involving both the π orbitals of the NIT radicals and the π orbitals of the central hfac$^-$ ligand (the one perpendicular to the O$_1$-O$_2$ direction, Figure 1). First, there is a charge transfer from the hfac$^-$ to the NIT radical that can relax by interacting with the local excitations on the NIT radical (from occupied to virtual MOs). Then, a second charge transfer operates from the other NIT radical to the hfac$^-$ orbitals. In the end, the operative exchange mechanism is not simply a classical super-exchange mechanism through the bridging hfac$^-$ ligand, but a more complex combination of this super-exchange with simultaneous stabilizing local excitations on the radical units.

Extension to complexes 2, 3a and 3b

Through-bond NIT–NIT interaction

In order to test the robustness of our *ab initio* approach, we have extended our study to the closely related complexes **2**, **3a** and **3b**, *i.e.* with a very similar coordination environment but highly different supramolecular arrangements. Evaluation of the magnetic coupling constants for the *through-bond* NIT–NIT interaction in compounds **2**, **3a** and **3b** has been

carried out using the same procedure as for compound **1**. The results are collected in Table 4. As expected, the J_{bond} values are all of the same order of magnitude. However, they can be separated in two groups: about -8.5 cm^{-1} for **1** and **3a** and about -10.2 cm^{-1} for **2** and **3b**. From the structural parameters (Tables S4 and S5), this difference can be explained by the slightly different NIT–NIT angle. For **1** and **3a**, this angle is about 140-145° while for **2** and **3b** it is close to 135°. The connexion between this angle and the value of J_{bond} can be analyzed in terms of orbital overlap: the larger this angle, the smaller the overlap between the orbitals of the NIT radical ligands and the hfac$^-$ ligand perpendicular to the O_1-O_2 direction (Scheme S1), and thus, the lower the antiferromagnetic contribution. From a purely theoretical point of view, this suggests that even larger values of J could be obtained by reducing the angle between the NIT radical ligands, a hardly predictable point from the synthetic point of view.

Table 4: *Through-bond* (J_{bond}) and *through-space* (J_{space}) calculated magnetic coupling constants (cm^{-1}) for complexes **1**, **2**, **3a** and **3b**. Experimental values are given for comparison. All the calculations are performed at the DDCI(2/2) level, using state average singlet 7:3 MOs.

Compound	J_{bond}	$J_{bond/exp}$	J_{space}	$J_{space/exp}$
1	-8.7	-15.6	-3.6	–
2	-10.2	-16.5	-0.5	–
3a	-8.5	-24.0	-178.0	-144.0
3b	-10.2	-18.5	19.6	–

Through-space NIT···NIT interaction

Regarding the *through-space* NIT···NIT interactions in **2**, **3a** and **3b**, only those where the NIT···NIT distance is smaller than 5 Å have been considered. As shown in Figure 8, only one *through-space* pathway has been investigated for each compound. Magnetic orbitals are shown in Figure 9.

For **2** and **3a**, the NIT interacting radicals adopt a head-to-tail conformation, as in **1**, but this time, they lie in almost parallel planes. The shortest inter-molecular NIT···NIT
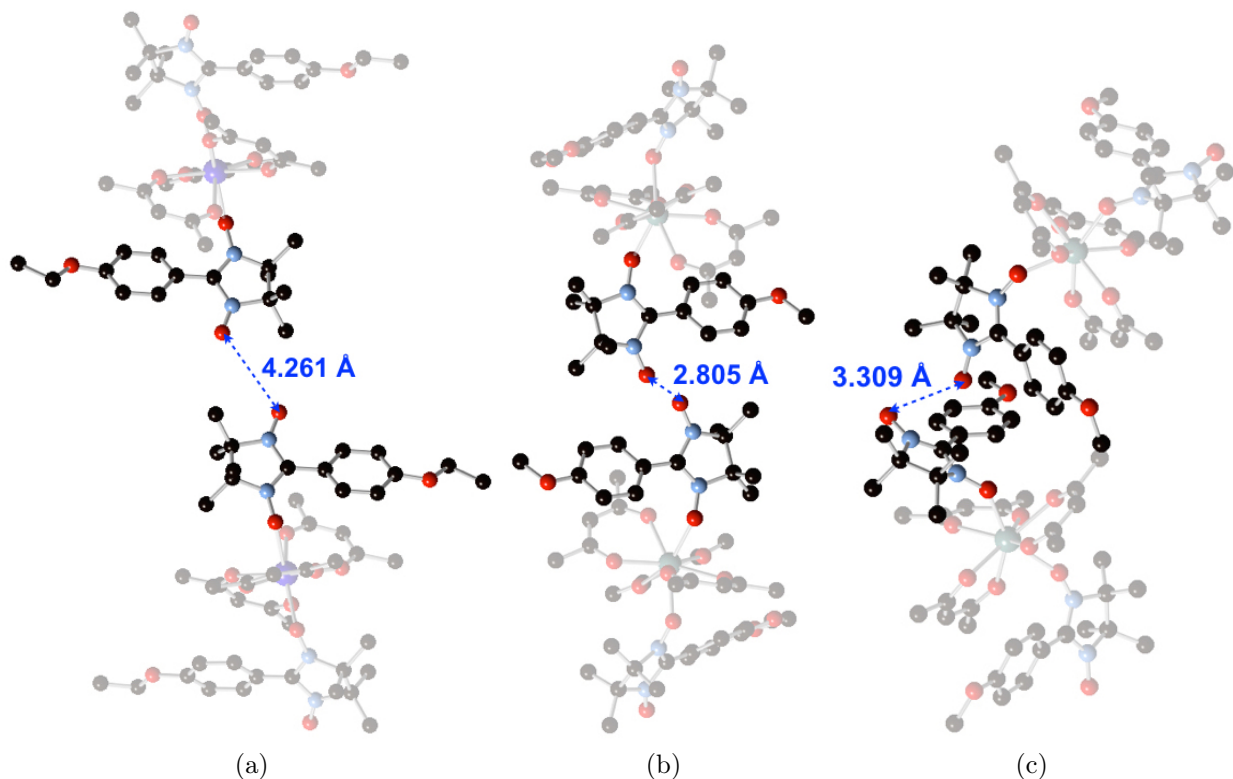
Figure 8: *Through-space* pathways (O$\cdots$O distances in blue) for **2** (a), **3a** (b) and **3b** (c).

distances are 4.261 Å and 2.805 Å for **2** and **3a**, respectively. For **2**, the calculated coupling is very weak (J_{space} = -0.5 cm^{-1}), as expected for such a large separation between the NIT units. From this, the Bleaney-Bowers model used experimentally seems to be appropriate to analyse the magnetic behavior of compound **2**. However, as for **1**, the magnetic curves can also be simulated by taking into account all the calculated magnetic interactions using the Hatfield model (Figure S8). Here again, the calculated J values have to be slightly corrected for a better agreement with experiment.

For **3a**, on the other hand, the *through-space* NIT$\cdots$NIT interaction is far from negligible since a strong antiferromagnetic interaction is found (J_{space} = -144 cm^{-1}, Table 4). This is undoubtedly related to the very short distance and the 180° between the planes containing the NIT radicals, that favors an efficient overlap between the π orbitals (Figure 9). Importantly, these results well support the experimental interpretation with a much larger *through-space* than *through-bond* interaction (Table 4).
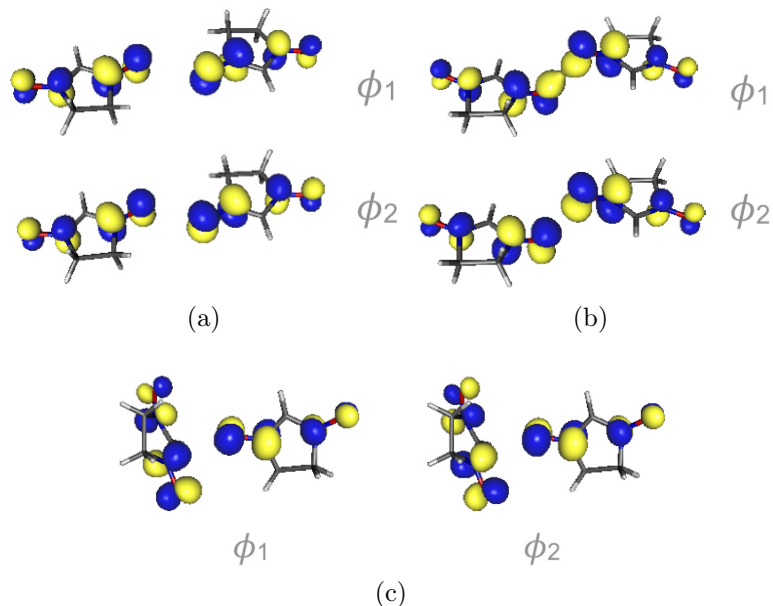
Figure 9: CAS(2,2)SCF SA-7:3 singlet MOs (ϕ_1 and ϕ_2) for the *through-space* NIT$\cdots$NIT interaction in **2** (a), **3a** (b) and **3b** (c).

For **3b**, as shown in Figure 8, the two interacting NIT radicals lie perpendicularly and the shortest inter-molecular NIT$\cdots$NIT distance is 3.309 Å. Here, the calculated interaction is found ferromagnetic with a J_{space} value of 19.6 cm^{-1} (Table 4). This quite large ferromagnetic interaction is induced by the orthogonality of the magnetic orbitals (Figure 9). Remarkably, this *through-space* NIT$\cdots$NIT interaction is of the same order of magnitude as the *through-bond* NIT–NIT interaction (J_{bond} = -10.2 cm^{-1}). Similarly to **1**, from the magnetic point of view, **3b** can thus be seen as a magnetic 1D chain with alternating interactions, but this time, with both ferromagnetic (intermolecular) and antiferromagnetic (intramolecular) interactions.[107] The curve simulated with these calculated J values (Figure S9) does not reproduce the experimental one as good as for **1** and **2**. However, this behavior was certainly expected for two well-separated reasons. From the computational point of view, it is well recognized that ferromagnetic interactions are often overestimated,[55] while experimentally, it has been evidenced (See Magnetic properties Section) that both **3b** and **3a** are always present in the samples.

4. Conclusions and perspectives

To conclude, through a combined theoretical and experimental investigation of a series of yttrium-based complexes containing NIT radicals, we show that *through-bond* and *through-space* NIT–NIT interactions can both be effective as soon as the inter-molecular NIT$\cdots$NIT distance remains smaller than 4-5 Å. This second interaction pathway strongly questions the up-to-now systematic use of the Bleaney-Bowers model to analyse the magnetic interactions in such complexes through fitting of the experimental data. Indeed, even if this model leads to a good quality fit, it does not give a realistic physical picture of the magnetic system. In this, state-of-the-art ab initio calculations, even if not fully quantitative, are the best tools to avoid loss of information but also potential over-parametrization.

Thanks to orbital localization procedures, we elucidate the microscopic mechanisms behind the *through-bond* NIT–NIT interaction, for which a predominant role is played by the π orbitals of the hfac$^-$ ligand orthogonal to the O_1-O_2 direction. Though, one should keep in mind that this mechanism might not hold similarly for the isostructural lanthanide derivatives of the $Y(hfac)_3(NIT-R)_2$ compounds studied here. Indeed, in other trivalent lanthanide ions, contrary to the Y(III) ion and even if shielded by the outer shells, the 4f orbitals are not empty and could be involved in the NIT–NIT interaction mechanisms, maybe through spin-polarization effects, as suggested by Benelli and Gatteschi,[46] but also through the empty 6s, 6p and 5d shells which have a larger radical expansion than the 4f shell. To support this hypothesis of non-transferability, one could refer to the work by Sutter and Kahn.[92–95] Using the HDVV Hamiltonian, they extract the coupling constant in isostructural Y(III), La(III) and Lu(III) complexes, which are all diamagnetic but with different electronic structures (empty 4f shell in Y(III) and La(III) while completely filled in Lu(III)). Surprisingly, the coupling constants are not identical for all complexes, suggesting different operating mechanisms. In addition, contrary to the mechanism evidenced here, most of the mechanisms discussed in the litterature for $Ln(hfac)_3(NITR)_2$ complexes involve either the half-filled 4f orbitals or the virtual 5d and 6s orbitals of the lanthanide ion.[25,27,34,43,46,47,92–95] To get a

clearer picture of the *through-bond* NIT–NIT interaction in these lanthanide derivatives, and clarify whether or not the lanthanide orbitals are involved in the exchange mechanism, we are currently investigating the Gd(III) analogue of **1**. Gd(III) is indeed a pure spin center and is thus expected to interact isotropically with the NIT radical ligands coordinated to it. This means that both the NIT–NIT and the Gd–NIT interactions can be described using the HDVV spin Hamiltonian.

Acknowledgement

References

1. Kahn, O. *Molecular Magnetism*; VCH, 1993.

2. Sessoli, R.; Gatteschi, D.; Caneschi, A.; Novak, M. A. Magnetic bistability in a metal-ion cluster. *Nature* **1993**, *365*, 141–143.

3. Gatteschi, D.; Sessoli, R.; Villain, J. *Molecular Nanomagnets*; Oxford University Press, 2006.

4. Leuenberger, M. N.; Loss, D. Quantum computing in molecular magnets. *Nature* **2001**, *410*, 789–793.

5. Sanvito, S. Molecular spintronics. *Chem. Soc. Rev.* **2011**, *40*, 3336–3355.

6. Bogani, L.; Wernsdorfer, W. Molecular spintronics using single-molecule magnets. *Nature Materials* **2008**, *7*, 179–186.

7. Candini, A.; Klyatskaya, S.; Ruben, M.; Wernsdorfer, W.; Affronte, M. Graphene spintronic devices with molecular nanomagnets. *Nano Lett.* **2011**, *11*, 2634–2639.

8. Ferrando-Soria, J.; Moreno Pineda, E.; Chiesa, A.; Fernandez, A.; Magee, S. A.; Carretta, S.; Santini, P.; Vitorica-Yrezabal, I. J.; Tuna, F.; Timco, G. A. *et al.* A modular design of molecular qubits to implement universal quantum gates. *Nature Commun.* **2016**, *7*, 11377.

9. Liu, J.-L.; Chen, Y.-C.; Guo, F.-S.; Tong, M.-L. Recent advances in the design of magnetic molecules for use as cryogenic magnetic coolants. *Coord. Chem. Rev.* **2014**, *281*, 26–49.

10. Christou, G.; Gatteschi, D.; Hendrickson, D. N.; Sessoli, R. Single-Molecule Magnets. *MRS Bull.* **2000**, *25*, 66–71.

11. Gatteschi, G.; Sessoli, R. Quantum tunneling of magnetization and related phenomena in molecular materials. *Angew. Chem. Int. Ed.* **2003**, *42*, 268–297.

12. Bar, A. K.; Pichon, C.; Sutter, J.-P. Magnetic anisotropy in two- to eight-coordinated transition-metal complexes: Recent developments in molecular magnetism. *Coord. Chem. Rev.* **2016**, *308*, 346 – 380.

13. Waldmann, O. A criterion for the anisotropy barrier in single-molecule magnets. *Inorg. Chem.* **2007**, *46*, 10035–10037.

14. Pointillart, F.; Bernot, K.; Sessoli, R.; Gatteschi, D. Effects of 3d-4f magnetic exchange interactions on the dynamics of the magnetization of Dy^{III}-M^{II}-Dy^{III} trinuclear clusters. *Chem. Eur. J.* **2007**, *13*, 1602–1609.

15. Gysler, M.; El Hallak, F.; Ungur, L.; Marx, R.; Hakl, M.; Neugebauer, P.; Rechkemmer, Y.; Lan, Y.; Sheikin, I.; Orlita, M. *et al.* Multitechnique investigation of Dy_3 – implications for coupled lanthanide clusters. *Chem. Sci.* **2016**, *7*, 4347–4354.

16. Layfield, R. A. Organometallic single-molecule magnets. *Organometallics* **2014**, *33*, 1084–1099.

17. Woodruff, D. N.; Winpenny, R. E. P.; Layfield, R. A. Lanthanide single-molecule magnets. *Chem. Rev.* **2013**, *113*, 5110–5148.

18. Luis, F.; Martínez-Pérez, M. J.; Montero, O.; Coronado, E.; Cardona-Serra, S.; Martí-Gastaldo, C.; Clemente-Juan, J. M.; Sesé, J.; Drung, D.; Schurig, T. Spin-lattice relaxation via quantum tunneling in an Er^{3+}-polyoxometalate molecular magnet. *Phys. Rev. B* **2010**, *82*, 060403.

19. Pointillart, F.; Bernot, K.; Golhen, S.; Le Guennic, B.; Guizouarn, T.; Ouahab, L.; Cador, O. Magnetic memory in an isotopically enriched and magnetically isolated mononuclear dysprosium complex. *Angew. Chem. Int. Ed.* **2015**, *54*, 1504–1507.

20. Demir, S.; Jeon, l.-R.; Long, J. R.; Harris, T. D. Radical ligand-containing single-molecules magnets. *Coord. Chem. Rev.* **2015**, *289-290*, 149–176.

21. Sessoli, R.; Bernot, K. In *Lanthanides and actinides in molecular magnetism*; Layfield, R. A., Murugesu, M., Eds.; Wiley-VCH, 2015; pp 89–124.

22. Rinehart, J. D.; Fang, M.; Evans, W. J.; Long, J. R. Strong exchange and magnetic blocking in N_2^{3-}-radical-bridged lanthanide complexes. *Nature Chem.* **2011**, *3*, 538–542.

23. Rinehart, J. D.; Fang, M.; Evans, W. J.; Long, J. R. A N_2^{3-} radical-bridged terbium complex exhibiting magnetic hysteresis at 14 K. *J. Am. Chem. Soc.* **2011**, *133*, 14236–14239.

24. Meihaus, K. R.; Cordey, J. F.; Fang, M.; Ziller, J. W.; Long, J. R.; Evans, W. J. Influence of an Inner-Sphere K^+ Ion on the Magnetic Behavior of N_2^{3-} Radical-Bridged Dilanthanide Complexes Isolated Using an External Magnetic Field. *Inorg. Chem.* **2014**, *53*, 3099–3107.

25. Benelli, C.; Caneschi, A.; Gatteschi, D.; Pardi, L.; Rey, P.; Shum, D. P.; Carlin, R. L. Magnetic properties of lanthanide complexes with nitronyl nitroxides. *Inorg. Chem.* **1989**, *28*, 272–275.

26. Bogani, L. A perspective on slow-relaxing molecular magnets built from rare-earths and nitronyl-nitroxide building blocks. *J. Appl. Phys.* **2011**, *109*, 07B115.

27. Benelli, C.; Gatteschi, D. Magnetism of lanthanides in molecular materials with transition-metal ion and organic radicals. *Chem. Rev.* **2002**, *102*, 2369–2387.

28. Benelli, C.; Gatteschi, D. *Introduction to molecular magnetism: from transition metals to lanthanides*; Wiley-VCH, 2015.

29. Gupta, T.; Rajeshkumar, T.; Rajaraman, G. Magnetic exchange in Gd^{III}-radical complexes: method assessment, mechanism of coupling and magneto-structural correlations. *Phys. Chem. Chem. Phys.* **2014**, *16*, 14568–14577.

30. Zhu, M.; Li, C.; Wang, X.; Li, L.; Sutter, J.-P. Thermal magnetic hysteresis in a copper-gadolinium-radical chain compound. *Inorg. Chem.* **2016**, *55*, 2676–2678.

31. Zhu, M.; Mei, X.; Ma, Y.; Li, L.; Liao, D.; Sutter, J.-P. Nitronyl nitroxide-metal complexes as metallo-ligands for the construction of hetero-tri-spin (2p-3d-4f) chains. *Chem. Commun.* **2014**, *50*, 1906–1908.

32. Zhu, M.; Wang, J.; Yang, M.; Ma, Y.; Li, L. Slow magnetic relaxation in two-dimensional 3d-4f complexes based on phenyl pyrimidyl substituted nitronyl nitroxide radicals. *Dalton Trans.* **2015**, *44*, 9815–9822.

33. Wang, X.-F.; Hu, P.; Li, Y.-G.; Li, L.-C. Construction of nitronyl nitroxide-based 3d-4f clusters: structure and magnetism. *Chem. Asian J.* **2015**, *10*, 325–328.

34. Benelli, C.; Caneschi, A.; Gatteschi, D.; Pardi, L.; Rey, P. Linear-chain gadolinium(III) nitronyl nitroxide complexes with dominant next-nearest-neighbor magnetic interactions. *Inorg. Chem.* **1990**, *29*, 4223–4228.

35. Lascialfari, A.; Ullu, R.; Affronte, M.; Cinti, F.; Caneschi, A.; Gatteschi, D.; Rovai, D.; Pini, M.; Rettori, A. Indication for a chiral phase in the molecular magnetic chain Gd(hfac)$_3$NiTiPr by specific heat and μ^+SR measurements. *J. Magn. Magn. Mater.* **2004**, *272-276, Part 2*, 1052–1053.

36. Cinti, F.; Rettori, A.; Barucci, M.; Olivieri, E.; Risegari, L.; Ventura, G.; Caneschi, A.; Gatteschi, D.; Rovai, D.; Pini, M. *et al.* Evidence for a helical and a chiral phase transition in the magnetic specific heat. *J. Magn. Magn. Mater.* **2007**, *310*, 1460–1461.

37. Cinti, F.; Rettori, A.; Pini, M.; Mariani, M.; Micotti, E.; Lascialfari, A.; Papinutto, N.; Amato, A.; Caneschi, A.; Gatteschi, D. *et al.* Experimental validation of Villain's conjecture about magnetic ordering in quasi-1D helimagnets. *J. Magn. Magn. Mater.* **2010**, *322*, 1259–1261.

38. Bogani, L.; Sangregorio, C.; Sessoli, R.; Gatteschi, D. Molecular engineering for single-chain-magnet behavior in a one-dimensional dysprosium-nitronyl nitroxide compound. *Angew. Chem. Int. Ed.* **2005**, *44*, 5817–5821.

39. Bernot, K.; Bogani, L.; Caneschi, A.; Gatteschi, D.; Sessoli, R. A family of rare-earth-based single chain magnets: playing with anisotropy. *J. Am. Chem. Soc.* **2006**, *128*, 7947–7956.

40. Bernot, K.; Bogani, L.; Sessoli, R.; Gatteschi, D. [Tm^{III}(hfac)$_3$(NITPhOPh)]∞: a new member of a lanthanide-based single chain magnets family. *Inorg. Chim. Acta* **2007**, *360*, 3807–3812.

41. Bernot, K.; Luzon, J.; Caneschi, A.; Gatteschi, D.; Sessoli, R.; Bogani, L.; Vindigni, A.; Rettori, A.; Pini, M. G. Spin canting in a Dy-based single-chain magnet with dominant next-nearest-neighbor antiferromagnetic interactions. *Phys. Rev. B* **2009**, *79*, 134419.

42. Bernot, K.; Luzon, J.; Bogani, L.; Etienne, M.; Sangregorio, C.; Shanmugam, M.; Caneschi, A.; Sessoli, R.; Gatteschi, D. Magnetic anisotropy of dysprosium(III) in a low-symmetry environment: a theoretical and experimental investigation. *J. Am. Chem. Soc.* **2009**, *131*, 5573–5579.

43. Benelli, C.; Caneschi, A.; Gatteschi, D.; Rey, P. Structure and magnetic properties of a gadolinium hexafluoroacetylacetonate adduct with the radical 4,4,5,5-tetramethyl-2-phenyl-4,5,-dihydro-1H-imidazole 3-Oxide 1-Oxyl. *Angew. Chem. Int. Ed.* **1987**, *26*, 913–915.

44. Benelli, C.; Caneschi, A.; Gatteschi, D.; Pardi, L.; Rey, P. Structure and magnetic properties of linear-chain complexes of rare-earth ions (gadolinium, europium) with nitronyl nitroxides. *Inorg. Chem.* **1989**, *28*, 275–280.

45. Benelli, C.; Caneschi, A.; Gatteschi, D.; Pardi, L.; Rey, P. One-dimensional magnetism of a linear chain compound containing yttrium(III) and a nitronyl nitroxide radical. *Inorg. Chem.* **1989**, *28*, 3230–3234.

46. Benelli, C.; Caneschi, A.; Gatteschi, D.; Sessoli, R. Magnetic interactions and magnetic ordering in rare earth metal nitronyl nitroxide chains. *Inorg. Chem.* **1993**, *32*, 4797–4801.

47. Benelli, C.; Caneschi, A.; Gatteschi, D.; Pardi, L.; Rey, P. Magnetic properties and phase transitions in molecular based materials containing rare earth ions and organic radicals. *J. Appl. Phys.* **1993**, *73*, 5333–5337.

48. Champion, G.; Lalioti, N.; Tangoulis, V.; Arrio, M.-A.; Sainctavit, P.; Villain, F.; Caneschi, A.; Gatteschi, D.; Giorgetti, C.; Baudelet, F. *et al.* XMCD for monitoring exchange interactions. The role of the Gd 4f and 5d orbitals in metal-nitronyl nitroxide magnetic chains. *J. Am. Chem. Soc.* **2003**, *125*, 8371–8376.

49. Launay, J.-P.; Verdaguer, M. *Electrons in molecules: from basic principles to molecular electronics*; Oxford University Press, 2014.

50. Bolvin, H. An alternative approach to the g-matrix: theory and applications. *Chem. Phys. Chem.* **2006**, *7*, 1575–1589.

51. Chibotaru, L. F.; Ceulemans, A.; Bolvin, H. Unique definition of the Zeeman-splitting g tensor of a Kramers doublet. *Phys. Rev. Lett.* **2008**, *101*, 033003.

52. Chibotaru, L. F.; Ungur, L.; Soncini, A. The origin of nonmagnetic Kramers doublets

in the ground state of dysprosium triangles: evidence for a toroidal magnetic moment. *Angew. Chem. Int. Ed.* **2008**, *47*, 4126–4129.

53. Chibotaru, L. F.; Ungur, L. *Ab initio* calculation of anisotropic magnetic properties of complexes. I. Unique definition of pseudospin Hamiltonians an their derivation. *J. Chem. Phys.* **2012**, *137*, 064112.

54. Atanasov, M.; Aravena, D.; Suturina, E.; Bill, E.; Maganas, D.; Neese, F. First principles approach to the electronic structure, magnetic anisotropy and spin relaxation in mononuclear 3d-transition metal single molecule magnets. *Coord. Chem. Rev.* **2015**, *289-290*, 177–214.

55. Malrieu, J.-P.; Caballol, R.; Calzado, C. J.; de Graaf, C.; Guihéry, N. Magnetic interactions in molecules and highly correlated materials: physical content, analytical derivation, and rigorous extraction of magnetic Hamiltonians. *Chem. Rev.* **2014**, *114*, 429–492.

56. Maurice, R.; Graaf, C. d.; Guihery, N. Theoretical determination of spin Hamiltonians with isotropic and anisotropic magnetic interactions in transition metal and lanthanide complexes. *Phys. Chem. Chem. Phys.* **2013**, *15*, 18784–18804.

57. Ruamps, R.; Maurice, R.; de Graaf, C.; Guihéry, N. Interplay between local anisotropies in binuclear complexes. *Inorg. Chem.* **2014**, *53*, 4508–4516.

58. Iwahara, N.; Chibotaru, L. F. Exchange interaction between J multiplets. *Phys. Rev. B* **2015**, *91*, 174438.

59. Iwahara, N.; Chibotaru, L. F. New mechanism of kinetic exchange interaction induced by strong magnetic anisotropy. *Scientific Reports* **2016**, *6*, 24743.

60. Zheludev, A.; Barone, V.; Bonnet, M.; Delley, B.; Grand, A.; Ressouche, E.; Rey, P.; Subra, R.; Schweizer, J. Spin density in a nitronyl nitroxide free radical. Polarized

neutron diffraction investigation and ab initio calculations. *J. Am. Chem. Soc.* **1994**, *116*, 2019–2027.

61. Ressouche, E.; Boucherle, J.-X.; Gillon, B.; Rey, P.; Schweizer, J. Spin density maps in nitroxide-copper(II) complexes. A polarized neutron diffraction determination. *J. Am. Chem. Soc.* **1993**, *115*, 3610–3617.

62. Angeli, C.; Calzado, C. J.; de Graaf, C.; Caballol, R. The electronic structure of Ullman's biradicals: an orthogonal valence bond interpretation. *Phys. Chem. Chem. Phys.* **2011**, *13*, 14617.

63. Zhao, Q.-H.; Ma, Y.-P.; Du, L.; Fang, R.-B. Three novel rare-earth complexes with nitronyl nitroxide radical $[RE(hfac)_3(NITPhOCH_3)_2]$ $[RE = Gd^{III}, Y^{III}$ and $Er^{III}]$: synthesis, crystal structures and magnetic properties. *Trans. Met. Chem.* **2006**, *31*, 593–597.

64. Sheldrick, G. M. A short history of *SHELX. Acta Crystallographica Section A* **2008**, *64*, 112–122.

65. Altomare, A.; Burla, M. C.; Camalli, M.; Carrozzini, B.; Cascarano, G. L.; Giacovazzo, C.; Guagliardi, A.; Moliterni, A. G. G.; Polidori, G.; Rizzi, R. *EXPO*: a program for full powder pattern decomposition and crystal structure solution. *Journal of Applied Crystallography* **1999**, *32*, 339–340.

66. Sheldrick, G. M.; Schneider, T. R. SHELXL : High-Resolution Refinement. *Macromolecular Crystallography Part B* **1997**, 319–343.

67. Farrugia, L. J. *WinGX* and *ORTEP for Windows*: an update. *Journal of Applied Crystallography* **2012**, *45*, 849–854.

68. Miralles, J.; Daudey, J.-P.; Caballol, R. Variational calculation of small energy differences. The singlet-triplet gap in $[Cu_2Cl_6]^{2-}$. *Chem. Phys. Lett.* **1992**, *198*, 555–562.

69. Miralles, J.; Castell, O.; Caballol, R.; Malrieu, J.-P. Specific CI calculation of energy differences: Transition energies and bond energies. *Chem. Phys.* **1993**, *172*, 33–43.

70. CASDI package developed at the Laboratoire de Chimie et Physique Quantiques, Université Toulouse III - Paul Sabatier, Toulouse, France.

71. Ben Amor, N.; Maynau, D. Size-consistent self-consistent configuration interaction from a complete active space. *Chem. Phys. Lett.* **1998**, *286*, 211.

72. Aquilante, F.; De Vico, L.; Ferré, N.; Ghigo, G.; Malmqvist, P.-Å.; Neogrady, P.; Pedersen, T. B.; Pitoňák, M.; Reiher, M.; Roos, B. O. *et al.* MOLCAS 7: The next generation. *J. Comput. Chem.* **2010**, *31*, 224.

73. Bories, B.; Maynau, D.; Bonnet, M.-L. Selected excitation for CAS-SDCI calculations. *J. Comput. Chem.* **2007**, *28*, 632–643.

74. Roos, B. O.; Lindh, R.; Malmqvist, P.-A.; Veryazov, V.; Widmark, P.-O. Main group atoms and dimers studied with a new relativistic ANO basis set. *J. Phys. Chem. A* **2004**, *108*, 2851–2858.

75. Roos, B. O.; Lindh, R.; Malmqvist, P.-A.; Veryazov, V.; Widmark, P.-O. New relativistic ANO basis sets for transition metal atoms. *J. Phys. Chem. A* **2005**, *109*, 6575–6579.

76. Roos, B. O.; Lindh, R.; Malmqvist, P.-A.; Veryazov, V.; Widmark, P.-O.; Borin, A. C. New relativistic atomic natural orbital basis sets for lanthanide atoms with applications to the Ce diatom and LuF$_3$. *J. Phys. Chem. A* **2008**, *112*, 11431–11435.

77. Hay, P. J.; Thibeault, J. C.; Hoffmann, R. Orbital interactions in metal dimer complexes. *J. Am. Chem. Soc.* **1975**, *97*, 4884–4899.

78. Anderson, P. W. Antiferromagnetism. Theory of superexchange interaction. *Phys. Rev.* **1950**, *79*, 350.

79. Anderson, P. W. New approach to the theory of superexchange interactions. *Phys. Rev.* **1959**, *115*, 2–13.

80. Kahn, O.; Briat, B. Exchange interaction in polynuclear complexes. Part 1.-Principles, model and application to the binuclear complexes of chromium(III). *J. Chem. Soc., Faraday Trans. 2* **1976**, *72*, 268–281.

81. Anderson, P. W. In *Solid state physics: advances in research and applications*; Turnbull, F., Seitz, F., Eds.; Academic Press: New York, 1963; p 99.

82. Hu, P.; Zhang, C.; Gao, Y.; Li, Y.; Ma, Y.; Li, L.; Liao, D. Lanthanide-radical linear chain compounds based on 2,4,4,5,5-pentamethylimidazoline-1-oxyl-3-oxide: Structure and magnetic properties. *Inorg. Chim. Acta* **2013**, *389*, 136–140.

83. Calzado, C. J.; Angeli, C.; de Graaf, C.; Caballol, R. Analysis of the magnetic coupling in nitroxide organic biradicals. *Theor. Chem. Acc.* **2011**, *128*, 505.

84. Novoa, J. J.; Lafuente, P.; Deumal, M.; Mota, F. In *Magnetism: molecules to materials IV*; Miller, J. S., Drillon, M., Eds.; Wiley-VCH: Weinheim, 2003; Chapter 3, p 65.

85. Suaud, N.; Ruamps, R.; Guihéry, N.; Malrieu, J.-P. A strategy to determine appropriate active orbitals and accurate magnetic couplings in organic magnetic systems. *J. Chem. Theory Comput.* **2012**, *8*, 4127–4137.

86. Novoa, J. J.; Deumal, M.; Jornet-Somoza, J. Calculation of microscopic exchange interactions and modelling of macroscopic magnetic properties in molecule-based magnets. *Chem. Soc. Rev.* **2011**, *40*, 3182–3212.

87. Angeli, C.; Calzado, C. J. The role of the magnetic orbitals in the calculation of the magnetic coupling constants from multireference perturbation theory methods. *J. Chem. Phys.* **2012**, *137*, 034104.

88. Giner, E.; Angeli, C. Metal-ligand delocalization and spin density in the $CuCl_2$ and $[CuCl_4]^{2-}$ molecules: Some insights from wave function theory. *J. Chem. Phys.* **2015**, *124305*, 143.

89. Cabrero, J.; Calzado, C. J.; Maynau, D.; Caballol, R.; Malrieu, J.-P. Metal-ligand delocalization in magnetic orbitals of binuclear complexes. *J. Phys. Chem. A* **2002**, *106*, 8146.

90. Garcia, V. M.; Castell, O.; Caballol, R.; Malrieu, J.-P. An iterative difference-dedicated configuration interaction. Proposal and test studies. *Chem. Phys. Lett.* **1995**, *238*, 222–229.

91. Spivak, M.; Angeli, C.; Calzado, C.; de Graaf, C. Improving the calculation of magnetic coupling constants in MRPT methods. *J. Comp. Chem.* **2014**, *35*, 1665–1671.

92. Kahn, M. L.; Sutter, J.-P.; Gohlen, S.; Guinneau, P.; Ouahab, L.; Kahn, O.; Chasseau, D. Systematic investigation of the nature of the coupling between a Ln(III) ion (Ln = Ce(III) to Dy(III)) and its aminoxyl radical ligands. Structural and magnetic characteristics of a series of Ln(organic radical)$_2$ compounds and the related Ln(nitrone)$_2$ derivatives. *J. Am. Chem. Soc.* **2000**, *122*, 3413–3421.

93. Kahn, M. L.; Ballou, R.; Porcher, P.; Kahn, O.; Sutter, J.-P. Analytical determination of the Ln-aminoxyl radical exchange interaction taking into account both the ligand-field effect and the spin-orbit coupling of the lanthanide ion (Ln = Dy^{III} and Ho^{III}). *Chem. Eur. J.* **2002**, *8*, 525–531.

94. Sutter, J.-P.; Kahn, M. L.; Gohlen, S.; Ouahab, L.; Kahn, O. Synthesis and magnetic behavior of rare-earth complexes with N,O-chelating nitronyl nitroxide triazole ligands: example of a [Gd^{III}organic radical$_2$] compound with an S = 9/2 ground state. *Chem. Eur. J.* **1998**, *4*, 571–576.

95. Sutter, J.-P.; Kahn, M. L.; Kahn, O. Conclusive demonstration of the ferromagnetic nature of the interaction between Holmium(III) and aminoxyl radicals. *Adv. Mater.* **1999**, *11*, 863–865.

96. Benelli, C.; Caneschi, A.; Fabretti, A. C.; Gatteschi, D.; Pardi, L. Ferromagnetic coupling of gadolinium(III) ions and nitronyl nitroxide radicals in an essentially isotropic way. *Inorg. Chem.* **1990**, *29*, 4153–4155.

97. Maynau, D.; Evangelisti, S.; Guihéry, N.; Calzado, C. J.; Malrieu, J.-P. Direct generation of local orbitals for multireference treatment and subsequent uses for the calculation of the correlation energy. *J. Chem. Phys.* **2002**, *116*, 10060.

98. Calzado, C. J.; Ben Amor, N.; Maynau, D. Magnetic coupling constants of self-assembled Cu(II) [3x3] grids: alternative spin model from theoretical calculations. *Chem. Eur. J.* **2014**, *20*, 8979–8987.

99. Calzado, C. J. On the controversial fitting of susceptibility curves of ferromagnetic Cu(II) cubanes: insights from theoretical calculations. *Chem. Eur. J.* **2013**, *19*, 1254–1261.

100. Chang, C.; Calzado, C. J.; Ben Amor, N.; Sánchez-Marín, J.; Maynau, D. Multi-scale multireference configuration interaction calculations for large systems using localized orbitals: Partition in zones. *J. Chem. Phys.* **2012**, *137*, 104102.

101. Tenti, L.; Maynau, D.; Angeli, C.; Calzado, C. J. Highly efficient perturbative plus variational strategy based on orthogonal valence bond theory for the evaluation of magnetic coupling constants. Application to the trinuclear Cu(II) site of multicopper oxidases. *Phys. Chem. Chem. Phys.* **2016**, *18*, 18365–18380.

102. Calzado, C. J.; Cabrero, J.; Malrieu, J. P.; Caballol, R. Analysis of the magnetic coupling in binuclear complexes. I. Physics of the coupling. *J. Chem. Phys.* **2002**, *116*, 2728–2747.

103. Calzado, C. J.; Cabrero, J.; Malrieu, J. P.; Caballol, R. Analysis of the magnetic coupling in binuclear complexes. II. Derivation of valence effective Hamiltonians from an initio Cl and DFT calculations. *J. Chem. Phys.* **2002**, *116*, 3985–4000.

104. Calzado, C. J.; Angeli, C.; Taratiel, D.; Caballol, R.; Malrieu, J.-P. Analysis of the magnetic coupling in binuclear complexes. III. The role of the ligand to metal charge transfer excitations revisited. *J. Chem. Phys.* **2009**, *131*, 044327.

105. Rota, J.-B.; Calzado, C. J.; Train, C.; Robert, V. Microscopic origins of the ferromagnetic exchange coupling in oxoverdazyl-based Cu(II) complex. *J. Chem. Phys.* **2010**, *132*, 154702.

106. Calzado, C. J.; Angeli, C.; Caballol, R.; Malrieu, J.-P. Extending the active space in multireference configuration interaction calculations of magnetic coupling constants. *Theor. Chem. Acc.* **2010**, *126*, 185–196.

107. Borras-Almenar, J. J.; Coronado, E.; Curely, J.; Georges, R.; Gianduzzo, J. C. Alternating chains with ferromagnetic and antiferromagnetic interactions. Theory and magnetic properties. *Inorg. Chem.* **1994**, *33*, 5171–5175.

Graphical TOC Entry
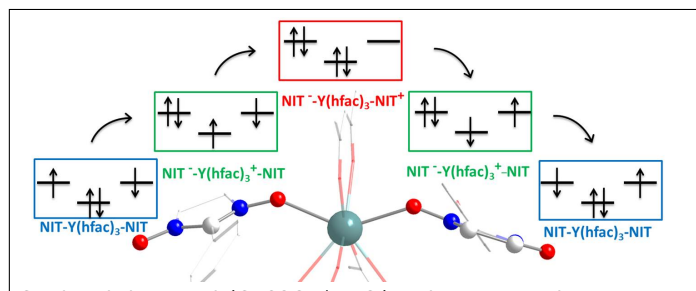
Combined theoretical (CASSCF/DDCI) and experimental investigations of a series of yttrium-based complexes containing nitronyl-nitroxide radicals (NIT) demonstrate that through-bond and through-space interactions can be effective for intermolecular distances as high as 5 Å. Orbital localization procedure highlights that π orbitals of hfac$^-$ ligands play a predominant role in mediating the through-bond NIT-NIT interaction.